

Journal Pre-proof

Sulfonamido carboranes as highly selective inhibitors of cancer-specific carbonic anhydrase IX

Jana Štěpánková, Michael Kugler, Josef Holub, Václav Šícha, Viswanath Das, Jan Někvinďa, Suzan El Anwar, Miroslav Havránek, Klára Pospíšilová, Milan Fábry, Vlastimil Král, Martina Medvedíková, Stanislava Matějková, Barbora Lišková, Soňa Gurská, Petr Džubák, Jiří Brynda, Marián Hajdúch, Bohumír Grüner, Pavlína Řezáčová



PII: S0223-5234(20)30431-1

DOI: <https://doi.org/10.1016/j.ejmech.2020.112460>

Reference: EJMECH 112460

To appear in: *European Journal of Medicinal Chemistry*

Received Date: 1 April 2020

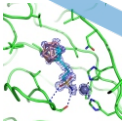
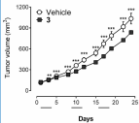
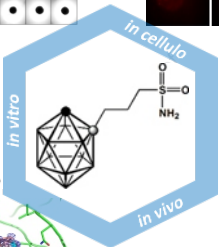
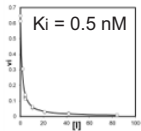
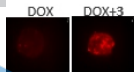
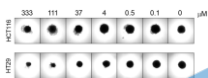
Revised Date: 8 May 2020

Accepted Date: 11 May 2020

Please cite this article as: J. Štěpánková, M. Kugler, J. Holub, Vá. Šícha, V. Das, J. Někvinďa, S. El Anwar, M. Havránek, Klá. Pospíšilová, M. Fábry, V. Král, M. Medvedíková, S. Matějková, B. Lišková, Soň. Gurská, P. Džubák, Jiří. Brynda, Mariá. Hajdúch, Bohumí. Grüner, Pavlí. Řezáčová, Sulfonamido carboranes as highly selective inhibitors of cancer-specific carbonic anhydrase IX, *European Journal of Medicinal Chemistry* (2020), doi: <https://doi.org/10.1016/j.ejmech.2020.112460>.

This is a PDF file of an article that has undergone enhancements after acceptance, such as the addition of a cover page and metadata, and formatting for readability, but it is not yet the definitive version of record. This version will undergo additional copyediting, typesetting and review before it is published in its final form, but we are providing this version to give early visibility of the article. Please note that, during the production process, errors may be discovered which could affect the content, and all legal disclaimers that apply to the journal pertain.

© 2020 Published by Elsevier Masson SAS.



Sulfonamido carboranes as highly selective inhibitors of cancer-specific carbonic anhydrase IX

Jana Štěpánková^{1,2,¥}, Michael Kugler^{3,4¥}, Josef Holub^{5¥}, Václav Šícha⁵, Viswanath Das^{1,2}, Jan Někviinda^{5,6}, Suzan El Anwar⁵, Miroslav Havránek⁷, Klára Pospíšilová⁴, Milan Fábry³, Vlastimil Král³, Martina Medvedíková¹, Stanislava Matějková⁴, Barbora Lišková¹, Soňa Gurská¹, Petr Džubák^{1,2}, Jiří Brynda^{3*}, Marián Hajdúch^{1,2,*}, Bohumír Grüner^{5*}, Pavlína Řezáčová^{4*}

Affiliations

¹ Institute of Molecular and Translational Medicine, Olomouc, Hněvotínská 1333/5, 77900 Olomouc, Czech Republic

² Cancer Research Czech Republic, Hněvotínská 5, 77900 Olomouc, Czech Republic

³ Institute of Molecular Genetics of the Czech Academy of Sciences, Flemingovo nam. 2, 16610 Prague, Czech Republic

⁴ Institute of Organic Chemistry and Biochemistry of the Czech Academy of Sciences, Flemingovo nam. 2, 16610 Prague, Czech Republic

⁵ Institute of Inorganic Chemistry of the Czech Academy of Sciences, 250 68 Řež, Czech Republic

⁶ Department of Organic Chemistry, Faculty of Natural Science, Charles University, Hlavova 2030, 12800 Prague 2, Czech Republic.

⁷ Apigenex, s.r.o. Poděbradská 59/ 186, 180 66 Prague 9, Czech Republic.

Corresponding Authors (*)

Dr. P. Řezáčová, E-mail: pavlina.rezacova@uochb.cas.cz, Phone: +420 220 183 144

Dr. B. Grüner, E-mail: gruner@iic.cas.cz, Phone: +420 311 236 942

Dr. M. Hajdúch, E-mail: marian.hajduch@upol.cz, Phone: +420 585 632 082

Dr. J. Brynda, E-mail: brynda@img.cas.cz, Phone: +420 220 183 210

(¥) These authors contributed equally.

Declaration of interest

The authors declare the following competing financial interest(s): B. G., J. B., V. S., J. H., P. D., M. H., and P. R. are inventors of a United States Patent, Pat. No. 9,290,529 B2, issued on Mar. 22, 2016, that covers the title compounds.

Journal Pre-proof

Abstract

Carbonic anhydrase IX (CA IX) is a transmembrane enzyme overexpressed in hypoxic tumors, where it plays an important role in tumor progression. Specific CA IX inhibitors potentially could serve as *anti-cancer* drugs. We designed a series of sulfonamide inhibitors containing carborane clusters based on prior structural knowledge of carborane binding into the enzyme active site. Two types of carborane clusters, 12-vertex dicarba-*closo*-dodecaborane and 11-vertex 7,8-dicarba-*nido*-undecaborate (dicarbollide), were connected to a sulfonamide moiety *via* aliphatic linkers of varying lengths (1 to 4 carbon atoms; $n = 1-4$). *In vitro* testing of CA inhibitory potencies revealed that the optimal linker length for selective inhibition of CA IX was $n=3$. A 1-sulfamidopropyl-1,2-dicarba-*closo*-dodecaborane (**3**) emerged as the strongest CA IX inhibitor from this series, with a K_i value of 0.5 nM and roughly 1,230-fold selectivity towards CA IX over CA II. X-ray studies of **3** yielded structural insights into their binding modes within the CA IX active site. Compound **3** exhibited moderate cytotoxicity against cancer cell lines and primary cell lines in 2D cultures. Cytotoxicity towards multicellular spheroids was also observed. Moreover, **3** significantly lowered the amount of CA IX on the cell surface both in 2D cultures and spheroids and facilitated penetration of doxorubicin. Although **3** had only a moderate effect on tumor size in mice, we observed favorable ADME properties and pharmacokinetics in mice, and preferential presence in brain over serum.

Keywords

anti-tumor agents; carbonic anhydrase IX; carboranes; dicarbollide; enzyme inhibitors; drug penetration; multicellular spheroids

Introduction

Hypoxia is a major contributor to tumor development and progression [1]. Growing tumors have an insufficient supply of oxygen, which leads to changes in cell metabolism such that glycolysis becomes the preferred pathway to metabolize glucose. This phenomenon, known as the Warburg effect [2], results in acidification of the extracellular environment, which promotes tumor cell invasiveness and increases resistance to chemotherapy and radiotherapy [3], [4]. Hypoxia stimulates overexpression of many proteins critical for cancer cell survival and metastases.

Carbonic anhydrase IX (CA IX) is one of the key proteins controlled by hypoxia-induced transcription factor (HIF). This membrane-bound enzyme catalyzes reversible hydration of carbon dioxide to bicarbonate in the extracellular space and plays an important role in tumor progression [5-7]. While physiological expression of CA IX is limited to the gastrointestinal tract [8], overexpression of CA IX has been reported in a broad spectrum of malignancies. CA IX overexpression indicates poor prognosis in lung, breast, cervical, brain, renal and neck cancers [9-14]. CA IX thus represents a clinically relevant biomarker and a target for development of anticancer drugs.

CA IX belongs to large group of human carbonic anhydrases, are ubiquitous zinc metalloenzymes with different subcellular localizations and tissue expression profiles. In addition to CA IX, several other isoforms are also recognized as therapeutic targets for the treatment of various diseases [15]. Development of inhibitors that selectively target CA IX has been a subject of intensive investigation [16], [17] [18]. Sulfonamides have shown potential as anticancer agents in preclinical experiments and clinical trials [19], [20]. A current challenge in the development of therapeutic agents targeting CA IX is designing compounds that specifically inhibit this isoenzyme and not the 11 other catalytically active human CA isoforms [21].

The isomeric dicarba-*closo*-dodecaboranes (with broadly used trivial name carboranes) are a newly emerging three-dimensional pharmacophores, providing hydrophobic interactions between biologically active molecules coupled to the boron cluster and their receptors [22]. Carboranes not only act as a space-filling moiety but also can increase a compound's interaction energy, *in vivo* stability and bioavailability [23, 24]. The use of carboranes as components of pharmacologically relevant molecules has rapidly been increasing [22-25, 26-28]. Previously, we introduced icosahedral dicarba-*closo*-dodecaborane, 11-vertex dicarba-*nido*-undecaborate (dicarborollide) and cobalt bis(dicarborollide) scaffolds into structures of sulfamide-type compounds

[29-31]. These cluster compounds exhibited inhibitory activity against CA IX in the micromolar to subnanomolar concentration range and showed promising selectivity [29-31]. Structural information about the active-site binding mode of these carborane inhibitors determined by X-ray diffraction aided further inhibitor design, leading to the compounds presented in this work.

Experiments with an organic series of inhibitors revealed that a sulfonamide head group can bind to the zinc atom present in the active center of the enzyme with higher interaction energy than a sulfamide [32]. Therefore, when considering further improvements in the structures of active carborane species, we replaced the sulfamide group [29] with a sulfonamide. Here, we present the synthetic procedure based on insertion of a newly prepared family of organic alkyne-1-sulfonamides into the open cage decaborane derivative, 6,9-(Me₂S)₂-*arachno*-B₁₀H₁₂. This yielded a series of 1,2-dicarba-*closo*-dodecaboranes substituted at the cage with alkylsulfonamide functions and enabled us to finely tune the length of the alkyl linker connecting both moieties. Also a series of 7,8-dicarba-*nido*-undecaborates was prepared in parallel by degradation of the cage of the respective 1,2-dicarba-*closo*-dodecaborane derivatives.

The aim of this work was to evaluate *closo*- and *nido*-dicarboranes substituted at the cage with alkylsulfonamide function as specific inhibitors of CA IX *in vitro*, *in cellulo* and *in vivo*. Our results show that the presence of alkylsulfonamide group led to significant improvements in *in vitro* inhibitory activity compared to a series of similar sulfamide compounds [30]. We also confirmed that the new compounds act as potent and specific inhibitors of CA IX *in vivo*. The selected lead compound of formula **1-H₂NSO₂C₃H₆-1,2-C₂B₁₀H₁₁ (3)** exhibited a tumor-specific growth inhibitory effect in both two-dimensional (2D) and multicellular spheroid (MCS) cultures of CA IX-positive cell lines. Compound **3** also showed favorable pharmacologic properties, as demonstrated using *in vitro* absorption, distribution, metabolism and excretion (ADME) assays and *in vivo* pharmacokinetics methods. In mouse models, this compound displayed anti-cancer effect in both syngenic breast (4T1-12B) and human xenografted HT-29 colorectal tumors.

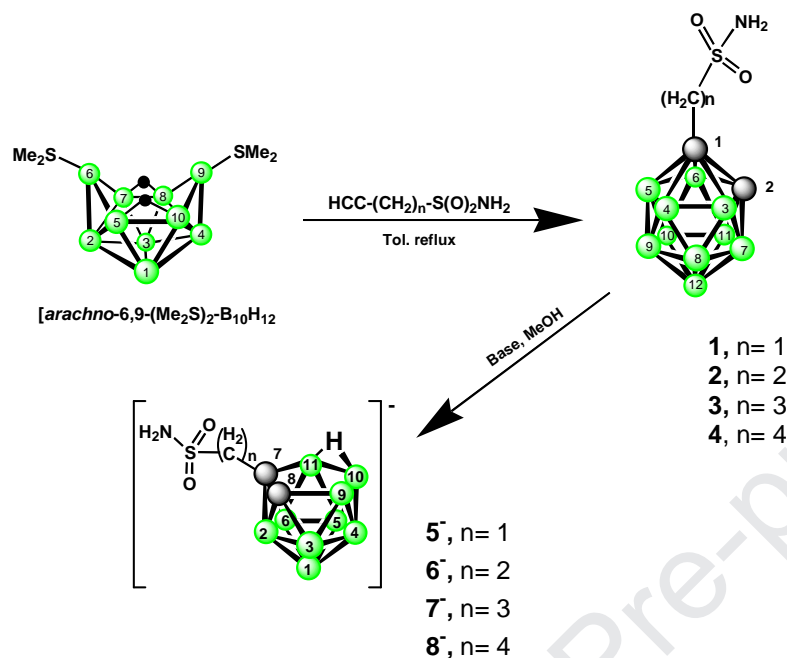
Results

Compound design and synthesis

General pathways to substituted 1,2-dicarba-*closo*-dodecaboranes usually involve incorporation of substituted alkynes into ten-vertex open-cage precursors [typically bis(ligand) derivatives of *nido*-decaborane(14), i.e. 6,9-(CH₃CN)₂-*arachno*-B₁₀H₁₂ or 6,9-(Me₂S)₂-*arachno*-B₁₀H₁₂ or lithiation of the CH groups in the 1,2-dicarba-*closo*-dodecaboranecage followed by reaction with numerous reagents [22] [25]. To our knowledge, no 1,2-dicarba-*closo*-dodecaborane derivatives with sulfonamide groups had been prepared to date. The still-limited availability of alkynes bearing terminal sulfonamide groups for insertion reactions, as well as the absence of reaction pathways for direct reactions, may account for the absence of such derivatives. The presence of polar sulfonamide groups in the starting reagents could in principle lead to degradations of the cage, producing open-cage products or interfering with the terminal H₂N- group using lithiated carborane. Surprisingly, insertion of alkyne-1-sulfonamides of the general formulation H₂NSO₂(CH₂)_nC≡C (n=1-4) into the open-cage, 10-vertex 6,9-(Me₂S)₂-*arachno*-B₁₀H₁₂ derivative proceeded smoothly. The reactions, carried out in toluene at high temperature, resulted in high yield conversion, and the respective 1-alkylsulfonamide-1,2dicarba-*closo*-dodecaboranesdicarbaboranes of general formula 1-H₂NSO₂(CH₂)_n-1,2-C₂B₁₀H₁₁ (**1-4**) were isolated in good yields after simple work-up. This consisted of extraction of crude products into diethyl ether, degradation of minor open-cage products with methanol under slightly acidic conditions, and final purification by chromatography (see Scheme 1; for details, see Experimental or Supporting Information). A key factor in the successful synthesis of these carboranes is the availability of alkyne-1-sulfonamides. Synthesis of these compounds from suitable building blocks, such as sodium prop-2-yne-1-sulfonate and iodo-alk-1-yne, was enabled by recent progress in chemistry of acetylenes. These precursors were converted in several reaction steps to acetylenes with terminal sulfonamide groups (for full experimental details, see Supporting Information).

[Scheme 1, color print]

Scheme 1: Overall reaction scheme leading to neutral 1- $\text{H}_2\text{NSO}_2(\text{CH}_2)_n$ -1,2-dicarba-*closo*-dodecaboranes and 7- $\text{H}_2\text{NSO}_2(\text{CH}_2)_n$ -7,8-dicarba-*nido*-undecaborate ions.



The chemical stability of the alkyl sulfonamide group in the 1,2-dicarba-*closo*-dodecaboranedicarbaborane derivatives resembles that of organic sulfonamide compounds. The terminal group withstands attacks by strongly acidic or basic reagents with no noticeable decomposition. This feature was employed to produce a series of substituted 11-vertex 7,8-dicarba-*nido*-undecaborate ions of the general formulation $[7\text{-H}_2\text{NSO}_2(\text{CH}_2)_n\text{-7,8-C}_2\text{B}_9\text{H}_{11}]^-$ ($n = 1\text{-}4$, **5⁻**–**8⁻**) by degradation of the cage with excess of potassium hydroxide in methanol. The degradation proceeds far more easily than in the case of the parent 1,2-dicarba-*closo*-dodecaborane cage and can be accomplished even in the presence of water in methanol (typically used for quenching of these reactions) or with aqueous alkaline solutions. For example, degradation of dicarbaborane **4** to the respective potassium salt of **5⁻** could be performed with 6% aqueous potassium hydroxide at 60 °C. Experimentally observed rates of degradation increased with the length of the linker. The products were isolated by dilution of the reaction mixtures with water, evaporation of methanol, washing of the resulting aqueous solution with diethyl ether, and extraction of the products into ethyl acetate. Alternatively, the 1,2-dicarba-*closo*-dodecaborane cage in these species could be also degraded by treatment with triethylamine in methanol or by potassium or cesium fluoride in methanol, following the procedures described in the literature

[33]. Notably, no derivatives of 7,8-dicarba-*nido*-7,8-undecaborate ion were observed (by LC-MS) in mouse serum after administration of substituted 1,2-dicarba-*closo*-dodecaboranesdodecaborane (**2** and **3**) for pharmacokinetics studies. Substitution with terminal alkylsulfonamide groups appreciably increased aqueous solubility compared to the parent series of 7,8-dicarba-*nido*-undecaborate(1-) ions. For biological assays, compounds were used in the form of potassium salts from synthesis or converted to sodium salts by metathesis.

Inhibition of CA activity

Candidate inhibitors were tested *in vitro* using a stopped-flow carbon dioxide hydration assay. To assess selectivity, we compared inhibition of two CA isoforms, the cancer-associated CA IX and the widespread CA II (Table 1, Figures 1, S1 and S2).

Table 1. *In vitro* inhibition of selected carbonic anhydrase isoenzymes.

Compound	K_i (CA II) [nM]	K_i (CA IX) [nM]	Selectivity Index ^[a]
1	494.4 ± 113.3	1136.0 ± 140.7	0.44
2	21.0 ± 2.3	22.8 ± 3.4	0.92
3	622.0 ± 177.4	0.506 ± 0.11	1229.3
4	870.1 ± 91.04	3.65 ± 0.64	238.4
5	63007 ± 28409	6545 ± 1625	9.6
6	60.69 ± 22.36	45.16 ± 5.73	1.34
7	1546 ± 385.9	1.178 ± 0.12	1312.4
8	333 ± 36.59	1.605 ± 0.38	207.5

^[a] Selectivity index is the ratio between K_i (CA II) and K_i (CA IX)

Inhibitory constants (K_i values) against CA IX ranged from micromolar to low nanomolar. The selectivity for CA IX over CA II also differed substantially among compounds. Most compounds were selective toward CA IX, with the exception of **1** and **2**. Compounds with long alkyl linkers connecting the sulfonamide moiety to the cluster showed high inhibitory activity against CA IX (with K_i values in the low nanomolar range). The optimal linker length for CA IX

affinity was $n=3$; compounds **3** and **7** inhibited CA IX with subnanomolar or nanomolar K_i values and selectivity indices over 1,000. Compounds with $n=4$ linker (**4** and **8**) retained nanomolar inhibitory potency toward CA IX but lost selectivity. In contrast, the optimal length for CA II affinity was $n=2$, although none of the compounds in our series was a low-nanomolar inhibitor of CA II.

[Figure 1, grayscale print]

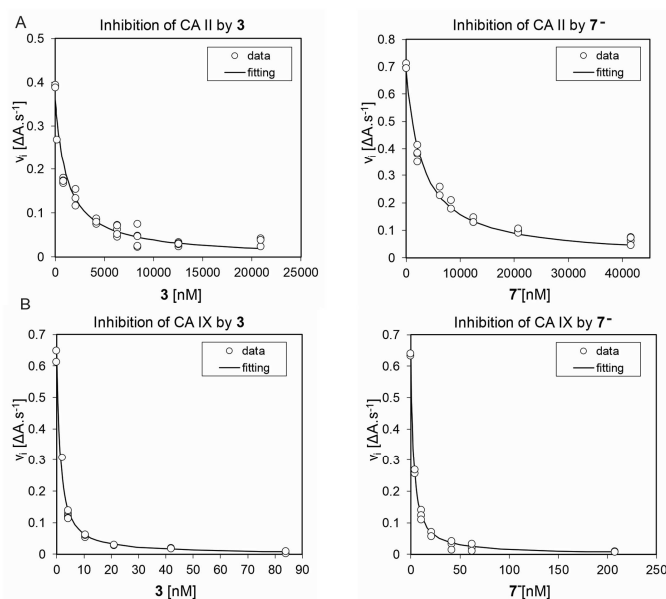


Figure 1. Inhibition of CA II (A) and CA IX (B) by rising concentration of compounds 3 and 7. Plots show the dose dependent decrease of CA catalytic activity of given. v_i is initial reaction rate (reaction rate is determined as 1st derivative of the absorbance with respect to time), each dot represents one measurement (some points are overlaid), black line shows fitted curves by the nonlinear least-squares method using Williams-Morrison equation. Raw data of absorbance change in the stopped-flow carbon dioxide hydration assay are shown in Figure S3.

Binding pose and interactions within the CA IX active site

The two compounds with the highest affinity and selectivity toward CA IX, **3** and **7**, were selected for structural studies to explore their interactions with the CA IX active site. Compounds were co-crystallized with a CA IX mimic - CA II containing seven amino acid substitutions in the active site (A65S, N67Q, E69T, I91L, F130V, K169E, and L203A). This variant is often used in structural studies because it retains the good crystallization properties of CA II while the active site resembles that of CA IX [34]. The K_i values for inhibition of CA IX mimic by **3** and **7** were 2.949 ± 0.48 nM and 17.25 ± 2.54 nM, respectively. These values are comparable to K_i values determined for inhibition of CA IX and differ substantially from K_i values for inhibition of CA II, indicating that CA IX mimic is indeed applicable to explore interactions of **3** and **7** with the CA IX active site. Two crystal structures determined at atomic resolutions of 1.1-1.2 Å confirmed specific binding of **3** and **7** in the CA IX active site (Figure 2A, B, Figure S4).

The sulfonamide moiety is deeply buried in the active site, where it makes polar interactions with the zinc ion and residues located at the bottom of the active site cavity (His94, His96, and His119). This binding mode is similar to interactions with the enzyme active site reported for organic sulfonamide-containing inhibitors [35-37]. In addition to interactions with catalytic residues, **3** made 19 interatomic interactions with H64, Q92, V121, L198, T199-200 and W209. Two additional contacts were observed for **7**, for a total of 21 interatomic interactions with Q92, V121, V131, V135, L198 and T199-200. The hydrophobic carborane clusters of **3** and **7** interact with a hydrophobic pocket formed by L91, V121, V131, V135, L141 and L198.

The linker moiety of **7** adopts an extended conformation, with second carbon in the aliphatic chain in transposition to N atom of sulfonamide group. The second and third carbon atoms in the aliphatic chain of **3** adopt a *gauche* conformation, and the second carbon atom in the chain is in *trans* to the O2 atom of the sulfonamide group (Figure 2C). We speculate that the extended conformation of **7** is caused by a polar interaction between the positive hydrogens of the amino groups of Q67, Q92 and negative charge of 7,8-dicarba-*nido*-undecaborate(1-) cage [38, 39].

[Figure 2, color print]

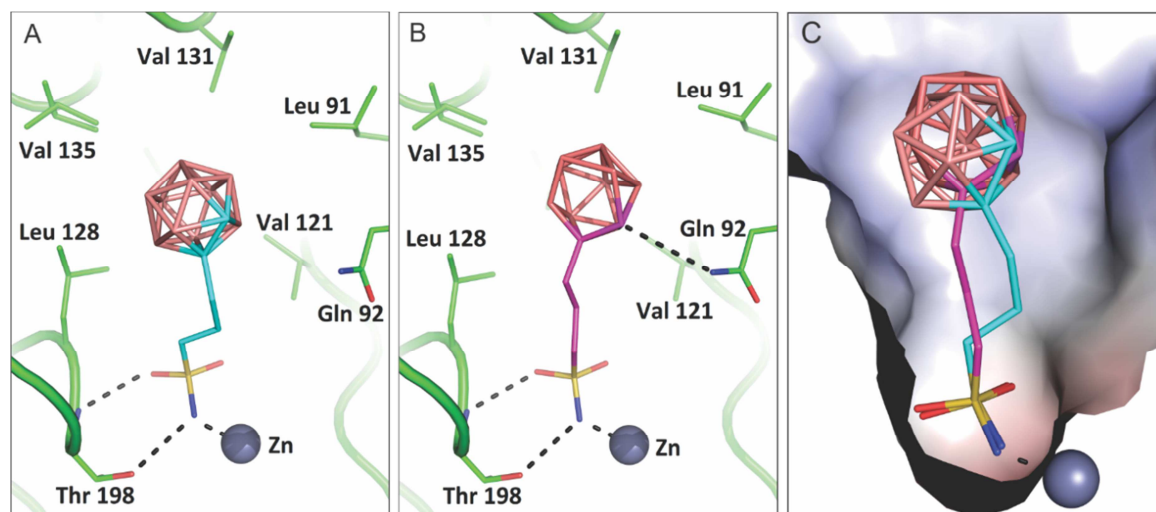


Figure 2. Structure of 3 (A) and 7 (B) bound to the CA IX active site. (A), (B) Compounds are depicted in stick representation, and the protein is shown in green cartoon representation with interacting residues highlighted as sticks and labelled. The Zn^{2+} ion is represented by a gray sphere. Dashed lines indicate polar interactions. (C) Overlay of the binding modes of **3** and **7** in the CA IX active site, which is represented by its solvent-accessible surface colored by electrostatic potential (red for negative, blue for positive).

Cytotoxicity of **3** in tissue cultures and spheroids

We assessed the toxicity of **3** in the form of a sodium salt on a panel of 11 cancer cell lines and two non-malignant fibroblast cell lines using a standard MTT assay under normoxic cell culture conditions. Compound **3** showed moderate cytotoxicity across the cell line panel, with no selectivity for malignant over non-malignant MRC-5 or BJ fibroblasts, possibly due to off-target effects (Table 2).

Table 2. Cytotoxicity of **3** in a panel of 13 cell lines. IC_{50} (μM) values are presented as mean \pm SD of four independent experiments.

MRC-5	BJ	CCRF-CEM	CEM-DNR	K562	K562-TAX	A549	HCT116	HT-29	HeLa	4T1-luc	MDCK-CAIX	MDCK-NEO
89±11	44±32	32±7	58±4	50±4	60±5	72±5	45±17	57±6	56±4	77±6	82±18	92±12

As spheroids of cancer cells mimic many characteristics of solid tumors [40], we next determined the effect of **3** on spheroids of HCT116 and HT-29 cells over a period of 3-7 days. In parallel, we determined the cytotoxicity of **3** after 7 days of treatment under normoxic conditions in 2D cultures of HCT116 and HT-29 cells by standard MTT assay. We observed a dose-dependent decrease in the size of MCSs of both the cell lines; the fold change in IC₅₀ values was more pronounced in MCSs of HT-29 cells (Figure 3). Similar to the 3D culture effect, longer treatment with **3** resulted in greater cytotoxicity in 2D cultures.

[Figure 3, color print]

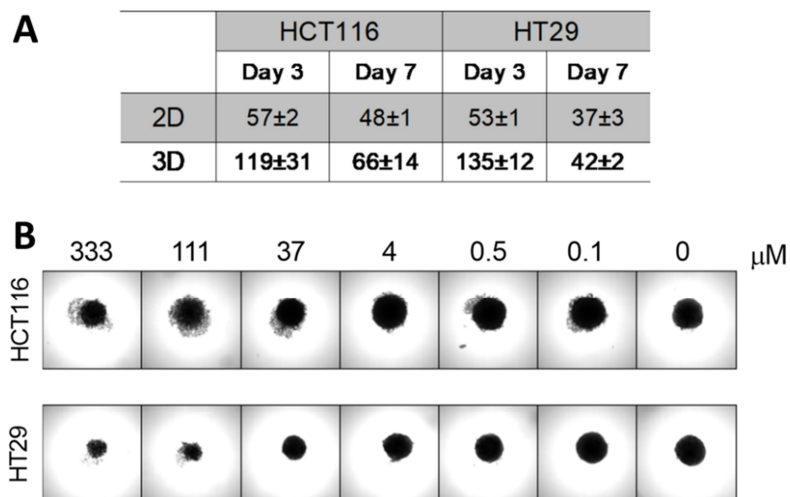


Figure 3. Effect of **3 on spheroid size.** (A) IC₅₀ values of **3** in 2D and spheroid cultures of HCT116 and HT-29 cells following 3-7 days of treatment under normoxic conditions. Data are

the mean \pm SEM, n = 3-4 independent experiments. (B) Images showing the dose-dependent effect of **3** in spheroids. Scale bar: 500 μ m.

Journal Pre-proof

Inhibition of CA IX expression in hypoxic 2D cultures and spheroids of HT-29

Previously, we found that some carborane sulfamide compounds affect both the amount and localization of intracellular CA IX. Specifically, CA IX was detected in high amounts in the cytoplasm and nuclei following treatment of HT-29 cells with 1-sulfamidoethyl derivative of cobalt bis(1,2-dicarbollide) ion [31].

To determine if **3** inhibits CA IX expression, 2D cultures of HT-29 cells were first grown under 1% O₂ for 4-5 days and then treated with different concentrations of **3** for 12 h in hypoxic conditions. We observed dose-dependent inhibition of transmembrane expression of CA IX by **3** (Figure 4A).

MTT assay indicated that the cytotoxic effect of **3** was more pronounced under when cells were treated for 72 h of treatment in hypoxia (Figure 4B). Although there was some cytotoxicity at 100 µM after 12 h, the decrease presence of cells in Fig. 4A after treatment with 50-100 µM **3** could be due to cell lifting from slides as CA IX downregulation has been reported to affect cell attachment [41]. Nevertheless, nuclear shrinkage presumably indicates the induction of cell death.

Similar to our findings in 2D cultures, treatment of HT-29 spheroids for 3 days with an IC₅₀ concentration of **3** inhibited the transmembrane expression of CA IX (Figure 4C). Furthermore, Western blot analysis of protein lysates from drug-treated spheroids indicated concentration-dependent inhibition of CA IX by **3** (Figure 4D).

Redistribution of CA IX may affect the composition of the extracellular matrix *via* modulation of matrix metalloproteinases activities [42] resulting in aberrant penetration of cytotoxic drugs into tissues [43].

[Figure 4, color print]

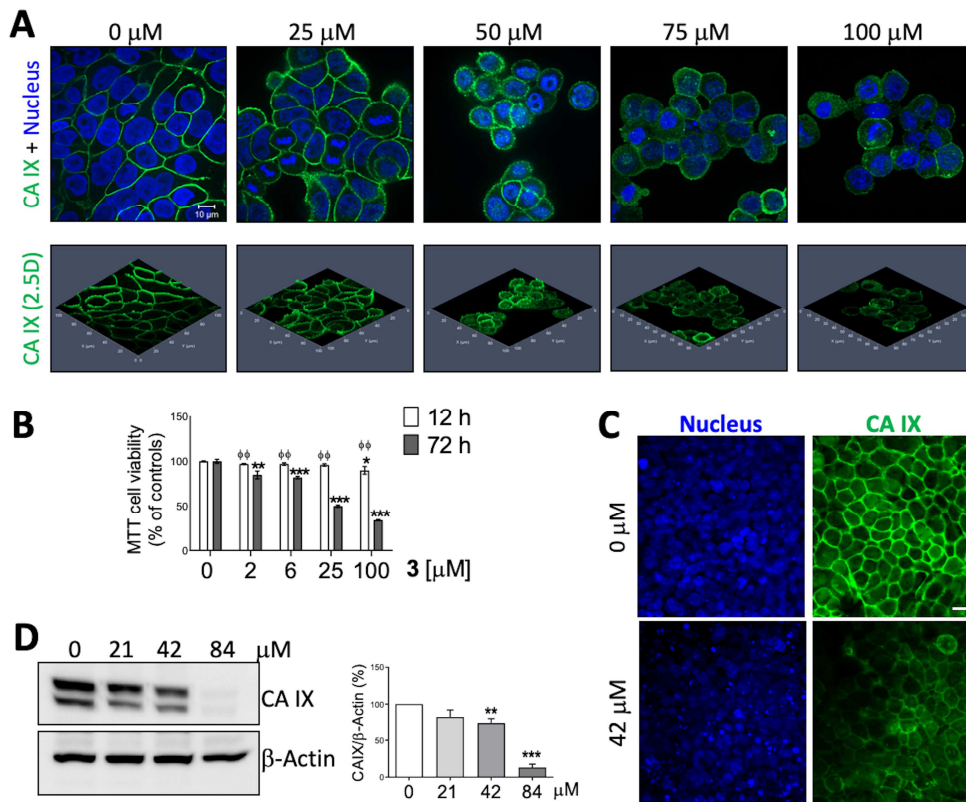


Figure 4. Treatment with 3 decreases CA IX expression in HT-29 cells. (A) Images showing CA IX expression in 2D cultures of HT-29 cells treated with **3** (100 μM) for 12 h under hypoxic (1% O_2) conditions. Scale bar: 10 μm . (B) MTT cell proliferation assay after treatment of 2D cultures of HT-29 cells with the indicated concentrations of **3** for 12-72 h in hypoxia. Data are mean \pm SEM of 3 independent experiments, *** $p < 0.001$, ** $p < 0.01$, * $p < 0.05$ comparing drug-treated to untreated (0 μM), one-way ANOVA with Dunnett's multiple comparison test; $\phi\phi$ $p < 0.01$ comparing 12 h to 72 h, unpaired t -test with Welch's correction. (C) Ten-day-old spheroids of HT-29 cells treated with **3** (42 μM) under standard cell culture conditions for 72 h show a decrease in CA IX expression. Scale bar: 50 μm . (D) Western blot showing a concentration-dependent decrease in the expression of CA IX in HT-29 spheroids following 72 h of treatment under standard conditions. Data are mean \pm SEM of 3 independent experiments, *** $p < 0.001$, ** $p < 0.01$ comparing treated to untreated, one-way ANOVA with Dunnett's multiple comparisons test.

Compound 3 facilitates doxorubicin accumulation in spheroids

Our recent study showed that ionic sulfamide derivatives of cobalt bis(1,2-dicarbollide) causing redistribution of CA IX also facilitated penetration of anti-cancer drugs such as doxorubicin (DOX) into spheroids [31]. Therefore, we next evaluated the penetration and accumulation of fluorescent DOX in spheroids following co-treatment with DOX and **3** for 140 min. Our live-spheroid imaging data revealed that also neutral compound **3** significantly increases the time-dependent penetration of DOX in co-treated spheroids compared with spheroids treated with DOX only (Figure 5A, B). Analysis of spheroids at a depth of 50 μm z-plane height showed increased accumulation of DOX in the interior of spheroids co-treated with DOX and **3** (Figure 5C). Tumor pH has been suggested to affect the intake of weakly basic anti-cancer drugs such as DOX [44], [40]. Immunostaining of drug-treated spheroids showed a marked decrease in CA IX level in the interior of spheroids at a depth of around 50 μm z-plane height (Figure 5D), suggesting that **3**-mediated inhibition of CA IX and potential alterations in pH facilitated DOX penetration into spheroids. The accumulation of DOX could also result due to cell death by **3**, causing increased permeabilization of DOX into dying cells. Additionally, the effect of **3** on CA IX may alter the composition of the extracellular matrix *via* modulation of matrix metalloproteinases activities [45], facilitating DOX penetration. These potential mechanisms need to be investigated in future studies.

[Figure 5, color print]

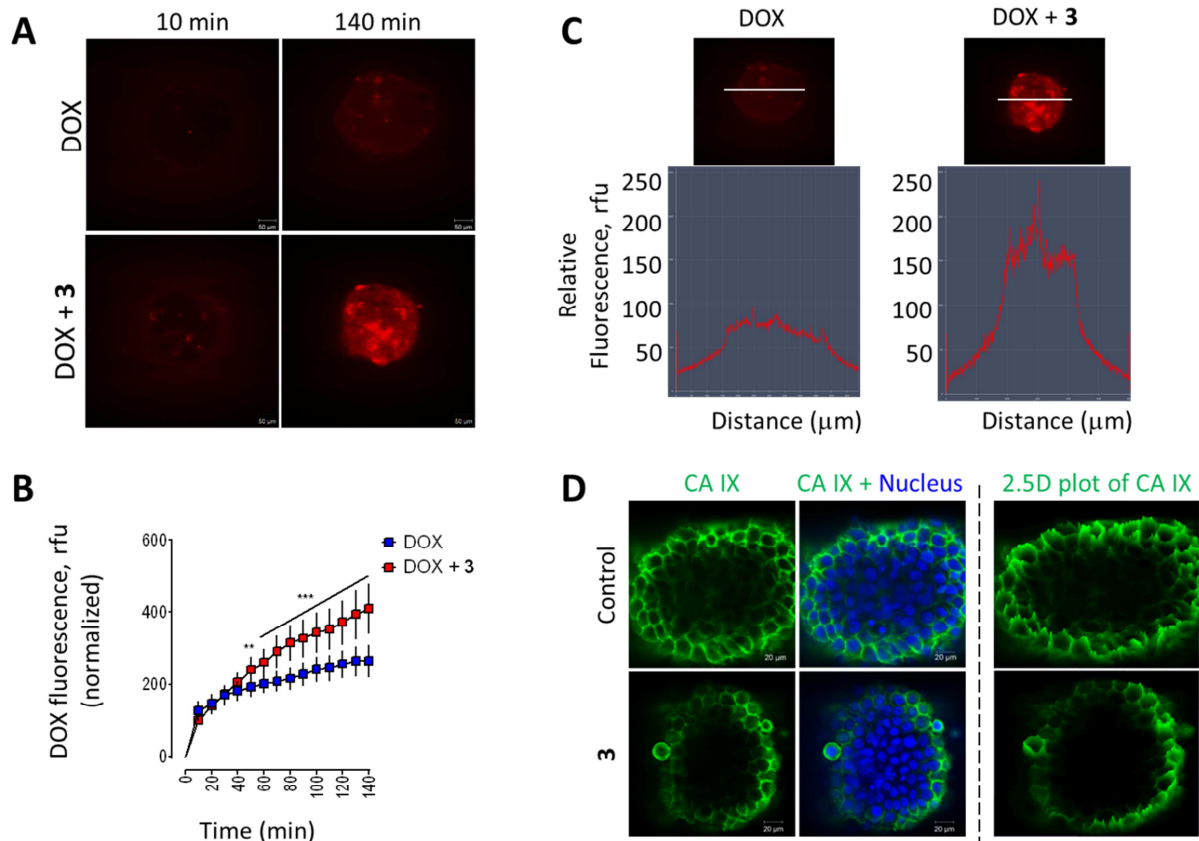


Figure 5. Concomitant treatment with 3 increases DOX accumulation in spheroids. (A) Images of HT-29 spheroids at a depth of 50 μm z-plane height showing the accumulation of DOX at the indicated time points in the absence and presence of 3. Scale bar: 50 μm , Objective: 20 \times . (B) Graph showing the rate of DOX accumulation in spheroids treated with DOX only (blue) and DOX in the presence of 3 (red). Data are mean \pm SEM of at least 4 spheroids per treatment from 3 independent experiments, *** $p < 0.001$, ** $p < 0.01$ comparing DOX + 3 to DOX only, two-way ANOVA with Sidak's multiple comparisons test. (C) Line-profile plot from images from (A) showing an increased accumulation of DOX after 140 min of treatment in the interior of spheroids treated with 3 compared with DOX-only-treated spheroids. (D) Downregulation of CA IX expression in 3-treated spheroids at a depth of 50 μm z-plane height. A 2.5D plot of spheroids shows a decrease in the CA IX expression in the interior of 3-treated spheroids compared with controls. Scale bar: 20 μm , Objective: 60 \times .

Pharmacological properties of compound 3

ADME parameters obtained from *in vitro* and *in vivo* assays indicated that the **3** is stable in plasma and binds more than 90% of plasma proteins (Table 3). The intrinsic clearance of **3** was classified as medium (in microsomal stability assay), and the compound was metabolized by microsomes with a half-time of 110 min. The transcellular permeation of **3** was classified as medium compared with other commonly used drugs in a parallel artificial membrane permeability assay (PAMPA) used as an *in vitro* model of passive diffusion. Furthermore, the medium permeability of **3** in Caco-2 cells indicates relatively good human intestinal permeability, suggesting that **3** would not be subject to drug efflux. Additionally, **3** showed a positive threshold for the central nervous system (CNS) and did not permeate MDCK-MDR1 cells, indicating a low potential for penetration through the blood-brain barrier.

Table 3. Pharmacological properties of **3** determined by *in vitro* and *in vivo* ADME assays

Metabolism			Permeability			
<i>in vitro</i>			<i>in vitro</i>		<i>in vivo</i>	
Plasma stability (category)	Plasma protein binding (% bound)	Microsomal stability (clearance)	PAMPA		MDR1-MDCK	Caco-2
			Category	% recovery	CNS (-ive/+ive)	Category
Stable	93.3%	Clearance category: Medium	Medium	log Pe: -5.8	CNS +ive	Moderate
					Papp (x10 ⁻⁶): 10.3	Papp (x10 ⁻⁶): 10
					Efflux ratio: 7.9	Efflux ratio: 0.2
					Active efflux: Yes	Active efflux: No
					% recovery: 38.8	% recovery: 82.4

Pharmacokinetics

The concentration-time profiles of **3** following intraperitoneal administration to NMRI mice at a maximum tolerated dose (MTD) of 125 mg/kg and ½ MTD of 62.5 mg/kg were determined over 36 h in plasma and brain. Besides initial symptoms of piloerection, there were no visible signs of drug toxicity on animal behavior, appearance, or body weight. Interestingly, we observed preferential penetration of **3** into the brain, with a peak 1 h after administration and a half-life of

2 h. While the maximum concentration (C_{\max}) of boron in serum was 75.1 μM , the C_{\max} in brain was 186 μM 1 h after administration of the MTD of **3** (Figure S5A, Table S2).

Brain penetration was not observed for previously studied family of metallacarborane sulfamide compounds (Figure S5B, C). Thus, we set out to decipher whether the nature of the cluster is crucial for penetration through the blood-brain barrier by assessing the pharmacokinetics of three other compounds containing *closo*- or *nido*-dicarbaborane clusters (**2**, **6** and **7**). Compound **2** exhibited preferential brain penetration, to an even higher extent than **3**. The C_{\max} of **2** in brain was 695 μM at 1 h, while C_{\max} in serum was 462 μM (Figure S5D). The half-life of **2** in brain was 12 h. On the other hand, concentrations of **6** and **7** in the brain were low or negligible, and these compounds were found mainly in serum (Figure S5E, F, Table S2). For **6**, the C_{\max} in serum was 2,997 μM at 0.5 h, while C_{\max} in brain was only 4.5 μM . Compound **7** reached a maximal serum concentration of 2,707 μM at 0.5 h, while C_{\max} in brain was 36 μM . These findings suggest that the presence of a dicarba-*closo*-dodecaborane cluster is essential for active transport into brain.

Antitumor activity of **3** in mouse models of mammary and colorectal tumors

We explored the *in vivo* anti-tumor activity of the sodium salt of **3** in two mouse models: (1) BALB/c mice bearing syngeneic mammary tumors of 4T1-12B cells and (2) SCID mice xenotransplanted with HT-29 cells (Figure 6). The effect of **3** on tumor size was evident in the first 10 days and after 29-30 days in BALB/c mice. In SCID mice, the effect of **3** on tumor size persisted throughout 24 days.

[Figure 6, grayscale print]

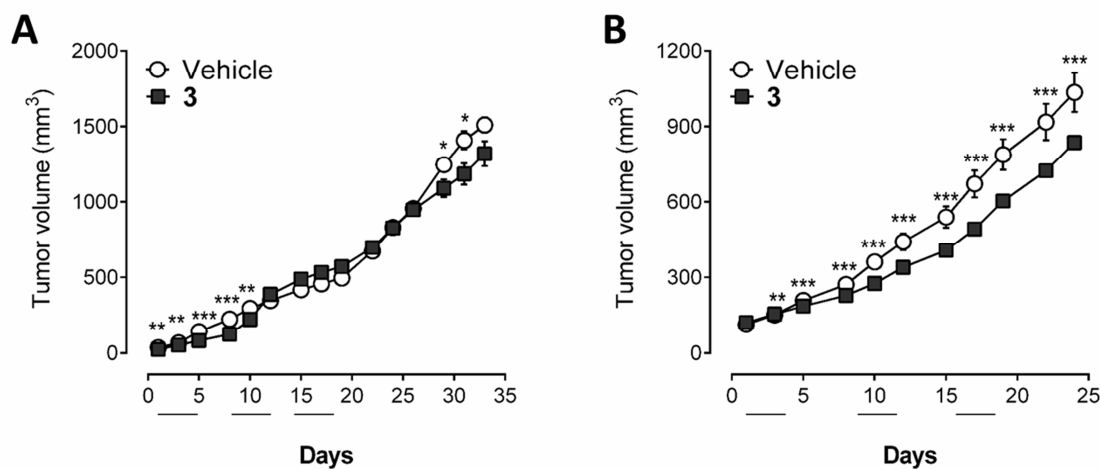


Figure 6. *In vivo* antitumor activity of **3**. Graphs showing the effect of **3** on tumor size in female (A) BALB/c mice orthotopically transplanted with 4T1-12B cells for 33 days and (B) SCID mice bearing subcutaneously transplanted HT-29 cell tumors for 24 days. Mice were administered **3** twice per day at a dose of 62.5 mg/kg. Dosing schedules are indicated by the black solid lines on the x-axes. Data in (A) and (B) are mean \pm SEM of typically 20 tumors transplanted to 10 animals per group, *** $p < 0.001$, ** $p < 0.01$, * $p < 0.05$ comparing vehicle-treated to drug-treated tumors, Student's *t*-test, paired.

Conclusions

We developed highly potent inhibitors of human carbonic anhydrase by using a structure-assisted design strategy and applying our previous knowledge of sulfamide compounds containing icosahedral dicarbaborane, 11-vertex dicarba-*nido*-undecaborate(1-) [30] and cobalt bis(dicarbollide)(1-) scaffolds [31]. By replacing the head group with alkylsulfonamide and varying the linker between the head group and carborane clusters, we fine-tuned inhibitor selectivity toward the cancer-specific CA IX isoform. These efforts led to an inhibitor with a subnanomolar inhibition constant and high selectivity (K_i value of 0.5 nM and selectivity index of 1,230 for CA IX over CA II). Atomic-resolution X-ray crystallographic structures uncovered interactions in active site of CA IX that are crucial for this high affinity and selectivity.

Of the various compounds generated in this series, we identified **3** as a promising candidate for further evaluation of activity in tissue cultures and spheroids. This compound exhibited moderate cytotoxicity against cancer cell lines and primary cell lines in 2D cultures, as

well as MCSs. Moreover, **3** significantly lowered the amount of CA IX on the cell surface both in 2D cultures and MCSs, facilitating the penetration of doxorubicin.

Compound **3** showed favorable ADME properties and pharmacokinetics in mice, CNS-positive properties in MDCK-MDR1 permeability assay indicating a greater potential for uptake across the blood-brain barrier and presence in the brain over serum. Although just moderate effect on tumor size in two mouse models (syngeneic and xenotransplanted tumors) was observed, we believe that compound **3** has a potential for future synergistic combinations to combat human cancers.

In conclusion, 1-sulfonamidopropyl-1,2-dicarbododecaboranes are highly selective inhibitors of cancer-specific carbonic anhydrase IX *in vitro* as well as *in vivo* and show thus the potential for further development of antitumor agents.

EXPERIMENTAL

Chemical syntheses. *Nido*-decaborane(14) (**14**) was purchased from Katchem Ltd., Czech Republic. The *arachno*-6,9-(Me₂S)₂-*arachno*-B₁₀H₁₂ was prepared by reaction of decaborane in dimethyl sulfide, as described in the literature [46]. Toluene was dried with sodium metal and distilled prior to use. Acetonitrile was dried using 4 Å molecular sieves (Fluka). Other chemicals were purchased from Aldrich. Solvents were obtained from Aldrich, Lachema a.s. and Penta Ltd., Czech Republic, and used without further purification. Analytical TLC was carried out on Silufol[®] (silica gel on aluminum foil, starch as binder, Kavalier, Czech Republic). Unless otherwise specified, column chromatography was performed on high-purity silica gel (Merck Grade, Type 7754, 70-230 mesh, 60 Å).

All reactions were performed with standard vacuum or inert-atmosphere techniques. Some operations, including flash chromatography and crystallization, were carried out in air. Melting points were determined in sealed capillaries on a BÜCHI Melting Point B-545 apparatus and are uncorrected.

Instrumental techniques. ¹H and ¹¹B NMR spectroscopy was performed on a Varian Mercury 400^{Plus} Instrument. The spectra of all compounds were measured immediately after dissolution. NMR chemical shifts are given in ppm to high-frequency (low field) relative to F₃B·OEt₂ as the

external reference. Residual solvent ^1H resonances were used as internal secondary standards. Coupling constants $^1J(^{11}\text{B}-^1\text{H})$ were measured by resolution-enhanced ^{11}B spectra with a digital resolution of 2 Hz and are given in Hz.

NMR data are presented in the following format: ^{11}B NMR: ^{11}B chemical shifts $\delta(^{11}\text{B})$ (ppm), multiplicity, $J(^{11}\text{B}-^1\text{H})$ coupling constants in Hz. Peak assignment is based on $\{^{11}\text{B}-^{11}\text{B}\}$ COSY NMR spectroscopy and comparison with the spectrum of the parent ion **1** (for assignment of the unsubstituted ligand). ^1H NMR: chemical shifts $\delta(^1\text{H})$ are given in ppm, coupling constants $J(\text{H},\text{H})$ in Hz. $\delta(^{11}\text{B}\{^1\text{H}\})$ data are also presented, assignment is based on selectively decoupled $\delta(^1\text{H})\text{-}\{^{11}\text{B selective}\}$ NMR experiments.

Mass spectrometry. MS measurements were performed on a Thermo-Finnigan LCQ-Fleet Ion Trap instrument using Atmospheric Pressure Chemical Ionization of Electrospray Ionization (ESI) techniques. Negative ions were detected. Samples dissolved in acetonitrile (concentrations approx. $100\text{ ng}\cdot\text{ml}^{-1}$) were introduced to the ion source by infusion ($5\ \mu\text{L}\cdot\text{min}^{-1}$). Molecular ions $[\text{M}]^-$ were detected for all univalent anions and $[\text{M}-\text{H}]^-$ for neutral compounds as the base peaks in the spectra. Full agreement between the experimental and calculated isotopic distribution patterns was observed for all compounds. HRMS were measured using an Agilent 6230 LC-TOFMS spectrometer with ESI ionization. The isotopic distribution in the boron plot of all peaks was in perfect agreement with the calculated spectral pattern. The data are presented for the most abundant mass in the boron distribution plot (100%) and for the peak corresponding to the m/z value.

Elemental analyses. Elemental analyses were performed on a Thermo Scientific FlashSmart Organic Elemental Analyzer using a V_2O_5 catalyst weighted with the sample for combustion of the samples in oxygen. All compounds were dried for 12 h in vacuum at $80\ ^\circ\text{C}$ before elemental analyses.

General procedure used for the synthesis of 1-(sulfonamido)alkyl-1,2-dicarba-closo-dodecaboranes (1-4). To a mixture of the corresponding (C3-C7) alkyne-1-sulfonamide (**A-D**) (36 mmol) and *arachno*-6,9-(Me_2S)₂-*arachno*- $\text{B}_{10}\text{H}_{12}$ (9.8 g, 40.0 mmol), toluene (50 mL) was added with a syringe. The slurry was heated under stirring and refluxed for 24 h. After cooling to

room temperature, solvent was removed under reduced pressure, and products were extracted with diethyl ether (3x 40 mL). The organic extracts were separated by filtration or decantation, and the combined fractions were evaporated under reduced pressure. The crude products were treated overnight with MeOH (50 mL) acidified with few drops of HCl (3 M) under stirring. The solvent was then evaporated to dryness. The methyl ester of boric acid formed from degradable open-cage impurities was removed by evaporation in this step. Pure products were isolated by liquid chromatography on a silica gel column (25 x 3.5 cm I.D.) using diethyl ether as a solvent. Fractions containing the product (according to NMR) were combined, evaporated under reduced pressure, and dried in a vacuum.

1-H₂NSO₂CH₂-closo-1,2-C₂B₁₀H₁₁; (1) white solid, yield: 5.71 g (67%); m.p. 143-145 °C, ¹¹B NMR (128 MHz, CD₃CN, 25 °C, BF₃.Et₂O): δ = -2.86 d (1B, J = 153, B(12)H), -4.67 d (1B, J = 153, B(9)H), -9.71 d (2B, J = 153, B(8,10)H), -11.00 d (2B, J = 104, B(7,11)H), -11.75 d (2B, J = 107, B(3,6)H), -13.04 d (2B, J = 162, B(4,5)H); ¹H {¹¹B} NMR (400 MHz, CD₃CN, 25 °C, TMS): δ = 5.69 br. s (2H, NH₂), 4.46 s (1H, C(2)H_{carborane}), 3.99 s (2H, CH₂S), 2.51 s (2H, B(3,6)H), 2.26 s (2H, B(7,11)H), 2.22 s (1H, B(12)H), 2.14 s (1H, B(9)H), 2.12 s (4H, B(4,5,8,10)H); ¹³C NMR (100 MHz, CD₃CN, 25 °C, TMS): δ = 68.24 s (1C, (1)_{carborane}), 61.80 d (1C, J = 194, C(2)H_{carborane}), 59.23 t (1C, J = 142, CH₂S); MS (HR ESI), m/z 236.1750 (100%) [M-H]⁻, 238.1677 (38%), calcd. 238.1681 for C₃H₁₄O₂N₁B₁₀S (38%); Analysis: Found C 15.53, H 6.35, N 5.78 Calcd. for B₁₀C₃H₁₅O₂NS: C 15.18; H 6.37, N 5.90.

1-H₂NSO₂(CH₂)₂-closo-1,2-C₂B₁₀H₁₁; (2) white solid, yield: 5.18 g (57%) m.p. 153-159 °C; ¹¹B NMR (128 MHz, CD₃CN, 25 °C, BF₃.Et₂O): δ = -3.03 d (1B, J = 146, B(12)H), -6.00 d (1B, J = 143, B(9)H), -9.69 d (2B, J = 150, B(8,10)H), -11.90 d (4B, J = 150, B(3,6,7,11)H), -13.04 d (2B, J = 156, B(4,5)H); ¹H {¹¹B} NMR (400 MHz, CD₃CN, 25 °C, TMS): δ = 5.37 br. s (2H, NH₂), 4.28 s (1H, C(2)H_{carborane}), 3.21 2d (2H, J = 12.8, CH₂S), 2.71 2d (2H, J = 12.4, CH₂), 2.33 s (2H, B(3,6)H), 2.19 s (1H, B(12)H), 2.15 s (2H, B(7,11)H), 2.09 s (4H, B(4,5,8,10)H), 2.05 s (1H, B(9)H); ¹³C NMR (100 MHz, CD₃CN, 25 °C, TMS): δ = 74.07 s (1C, C(1)_{carborane}), 63.56 d (1C, J = 197, C(2)H_{carb}), 53.96 t (1C, J = 138, CH₂S), 32.44 t (1C, J = 133, C(1)CH₂); MS (HR ESI), m/z 250.1907 (100%) [M-H]⁻, 252.1834 (30%), calcd. 252.1838 (30% for

$C_4H_{16}O_2N_1B_{10}S$; **Analysis:** Found C 19.34, H 6.73, N 5.56; Calcd. for $B_{10}C_3H_{15}O_2NS$: C 19.11, H 6.82, N 5.57.

1-H₂NSO₂C₃H₆-closo-1,2-C₂B₁₀H₁₁; (3). Compound was prepared starting from pent-4-yne-1-sulfonamide, white solid, yield: 5.2 g (54%), m. p. 130-140 °C; ¹¹B NMR (128 MHz, CD₃CN, 25 °C, BF₃.Et₂O): δ = -3.10 d (1B, *J* = 150, *B*(12)H), -6.24 d (1B, *J* = 146, *B*(9)H), -9.90 d (2B, *J* = 153, *B*(8,10)H), -11.92 d (4B, *J* = 168, *B*(3,6,7,11)H), -13.20 d (2B, *J* = 165, *B*(4,5)H); ¹H {¹¹B} NMR (400 MHz, CD₃CN, 25 °C, TMS): δ = 5.30 br. s (2H, NH₂), 4.21 s (1H, C(2)*H*_{carb}), 2.98 t (2H, *J* = 8.0, CH₂S), 2.57 s (1H, *B*(12)H), 2.39 t (2H, *J* = 8.8, CH₂), 2.32 s (2H, *B*(3,6)H), 2.18 s (2H, *B*(7,11)H), 2.07 s (4H, 4,5,8,10)H), 2.03 s (1H, *B*(9)H), 1.92 m (2H, C(1)CH₂); ¹³C NMR (100 MHz, CD₃CN, 25 °C, TMS): δ = 76.26 s (1C, C(1)_{carb}), 63.33 d (1C, *J* = 195, C(2)*H*_{carb}), 54.00 t (1C, *J* = 137, CH₂S), 36.13 t (1C, *J* = 133, CH₂), 24.60 t (1C, *J* = 132, C(1)CH₂); **HR MS:** *m/z* 264.2063 (100%) [M-H]⁻, 266.1990 (25%), calcd. 266.1994 (25% for C₅H₁₈O₂N₁B₁₀S); **Analysis:** Found C 22.86, H 6.95, N 5.68 Calcd. for $B_{10}C_3H_{15}O_2NS$: C 22.63, H 7.22, N 5.28.

1-H₂NSO₂C₄H₈-closo-1,2-C₂B₁₀H₁₁ (4). Compound was prepared at a 10-fold lower scale starting from hex-5-yne-1-sulfonamide (0.55 g, 3.41 mmol) and 6,9-(Me₂S)₂-B₁₀H₁₂ (1.0 g, 4.08 mmol) in toluene (25 mL). The same general procedure was used for product isolation; white solid, **yield:** 0.60 g (63%), m.p. 115-118 °C, ¹¹B NMR (128 MHz, CD₃CN, 25 °C, BF₃.Et₂O): δ = -3.22 d (1B, *J* = 156, *B*(12)H), -6.38 d (1B, *J* = 146, *B*(9)H), -9.95 d (2B, *J* = 156, *B*(8,10)H), -11.78 d (4B, *J* = 178, *B*(3,6,7,11)H), -13.23 d (2B, *J* = 162, *B*(4,5)H); ¹H {¹¹B} NMR (400 MHz, CD₃CN, 25 °C, TMS): δ = 5.22 br. s (2H, NH₂), 4.16 s (1H, C(2)*H*_{carborane}), 3.00 m (2H, CH₂S), 2.29 m (2H, *J* = 8.2, CH₂), 2.17 s (1H, *B*(12)H), 2.16 s (4H, 3,6,7,11)H), 2.07 s (4H, *B*(4,5,8,10)H), 2.02 s (1H, *B*(9)H), 1.70 m (2H, *J* = 8.0 CH₂), 1.59 t (2H, *J* = 8.0, CH₂); ¹³C NMR (100 MHz, CD₃CN, 25 °C, TMS): δ = 68.15 s (1C, C(1)_{carb}), 59.69 d (1C, *J* = 195, C(2)*H*_{carb}), 59.50 t (1C, *J* = 137, CH₂S), 42.28 t (1C, *J* = 137, CH₂), 33.21 t (1C, *J* = 133, CH₂), 28.67 t (1C, *J* = 132, C(1)CH₂); **MS (ESI),** *m/z* 278.2222 (100%), 281.2151 (35 %), calcd. 281.2224 for C₆H₂₀O₂N₁B₁₀S (38%); **Analysis:** Found C 26.08, H 7.24, N 5.28 Calcd. for $B_{10}C_3H_{15}O_2NS$: C 25.79, H 7.58, N 5.01.

General procedure for the synthesis of potassium salts of 7-(sulfonamido)alkyl--dicarbano-7,8-undecaborates (5-7). To the respective 1-(sulfonamido)alkyl-1,2-dicarbano-7,8-undecaborane (10 mmol), MeOH (50 mL) was added, followed by addition of solid KOH (0.40 g, 100 mmol) in several portions under vigorous stirring. The methanol solution was stirred and heated at 60 °C for 6 h under reflux. Then, water (50 mL) was added and MeOH was evaporated under reduced pressure. The resulting aqueous solution was diluted with water (60 mL) and extracted with diethyl ether (2 x 20 mL) and ethyl acetate (4 x 25 mL). The ethyl acetate extracts were combined, water (10 mL) was added, and the solvents were evaporated under reduced pressure. Final products were purified by liquid chromatography on a silica gel column (25 x 2.5 cm I.D.) using a CH₂Cl₂-CH₃CN solvent mixture (3:1 to 2:1 b.v.) for elution. Fractions containing the product (according to NMR) were combined, evaporated under reduced pressure, and dried in a vacuum for 5 h at 45 °C.

[7-H₂NSO₂CH₂-nido-7,8-C₂B₉H₁₁]K (5⁻). white solid, yield: 2.28 g (86%), m. p. 120 °C (decomp.); ¹¹B (128 MHz, CD₃CN, 25 °C, BF₃.Et₂O): δ = -10.85 d (2B, J = 134, B(9,11)H), -14.01 d (1B, J = 174, B(4)H), -15.37 d (1B, J = 143, B(6)H), -19.22 d (2B, J = 119, B(2,5)H), -21.29 d (1B, J = 204, B(3)H), -33.00 d (1B, J = 125, B(10)H), -37.44 d (1B, J = 140, B(1)H); ¹H {¹¹B} NMR (400 MHz, CD₃CN, 25 °C, TMS): δ = 3.76 br. s (2H, NH₂), 3.32 d (1H, J = 14.8, CH₂S), 3.05 d (1H, J = 14.8, CH₂S), 2.09 s (1H, B(9)H), 2.08 s (2H, CH₂S), 2.06 s (1H, C(8)H_{carborane}), 1.95 s (1H, B(11)H), 1.64 s (1H, B(4)H), 1.28 s (1H, B(6)H), 1.22 s (1H, B(3)H), 1.13 s (1H, B(5)H), 1.01 s (1H, B(2)H), 0.44 s (2H, B(1)H), -0.01 s (1H, B(10)H), -2.69 s (1H, μ-H); ¹³C NMR (100 MHz, CD₃CN, 25 °C, TMS): δ = 65.05 t (1C, J = 139, CH₂S), 52.92 s (1C, C(7)_{carb}), 45.63 d (1C, J = 149, C(8)H_{carb}); HRMS (ESI), m/z [M]⁻: 226.1736 (100%), 228.1664 (32%), calcd. 228.1667 for C₃H₁₅O₂N₁B₉S (50%); Analysis for Et₃NH.5: Found C 32.56, H 9.24, N 8.76, Calcd. for B₁₀C₃H₁₅O₂NS: C 32.88, H 9.51, N 8.52.

[7-H₂NSO₂-(CH₂)₂-nido-7,8-C₂B₉H₁₁]K (6⁻). white solid, yield: 2.24 g (80%), m. p. 229-232 °C (decomp.); ¹¹B (128 MHz, CD₃CN, 25 °C, BF₃.Et₂O): δ = -11.33 d (2B, J = 134, B(9,11)H), -14.23 d (1B, J = 159, B(4)H), -16.61 d (1B, J = 134, B(6)H), -19.32 d (2B, J = 140, B(2,5)H), -22.00 d (1B, J = 150, B(3)H), -33.51 d (1B, J = 128, B(10)H), -37.39 d (1B, J = 140, B(1)H); ¹H {¹¹B} NMR (400 MHz, CD₃CN, 25 °C, TMS): δ = 5.16 s (2H, NH₂), 3.13 m (2H, CH₂) and 1.89

m (2H, CH₂C), 1.81 s (1H, B(9)H), 1.71 br. s (1H, C(8)H_{carborane}), 1.71 s (1H, B(11)H), 1.63 s (2H, CH₂), 1.28 s (1H, B(5)H), 1.15 s (2H, B(3,6)H), 0.98 s (1H, B(2)H), 0.79 s (1H, B(4)H), 0.39 s (1H, B(1)H), -0.06 s (1H, B(10)H), -2.82 s (1H, μ -H); ¹³CNMR (100 MHz, CD₃CN, 25 °C, TMS): δ = 57.76 s (1C, C(7)_{carborane}), 56.29 t (1C, J = 137, CH₂S), 46.28 d (1C, J = 108, C(8)H_{carborane}), 33.74 t (1C, J = 132, CH₂C); **HRMS (ESI), m/z [M]**: 241.1855 (100%), 242.1819 (47%), calcd. 242.1823 for C₄H₁₇O₂N₁B₉S (47%); **Analysis for Et₃NH.6**: Found C 34.66, H 9.42, N 8.48 Calcd. for B₁₀C₃H₁₅O₂NS: C 35.04, H 9.70, N 8.17.

[7-H₂NSO₂-(CH₂)₃-nido-7,8-C₂B₉H₁₁]K (7). white solid, yield: 2.71 g (92%), m. p. 312-314 decomp.; ¹¹B (128 MHz, CD₃CN, 25 °C, BF₃.Et₂O): δ = -11.42 d (2B, J = 134, B(9,11)H), -14.32 d (1B, J = 156, B(4)H), -17.25 d (1B, J = 156, B(6)H), -18.86 d (2B, J = 186, B(2,5)H), -22.22 d (1B, J = 146, B(3)H), -33.63 d (1B, J = 125, B(10)H), -37.53 d (1B, J = 137, B(1)H); ¹H {¹¹B} **NMR** (400 MHz, CD₃CN, 25 °C, TMS): δ = 5.23 s (2H, NH₂), 2.94 m (2H, CH₂S), 2.30 s (1H, C(8)H_{carborane}), 1.85 (2H, B(9,11)H), 1.81 m (2H, J = 0.02, CH₂), 1.67 m (2H, J = 0.02, CH₂), 1.53 s (1H, B(4)H), 1.12 s (1H, B(3)H), 1.11 s (1H, B(6)H), 1.00 s (2H, B(2,5)H), 0.37 s (2H, B(1)H), -0.08 s (1H, B(10)H), -2.82 s (1H, μ -H); ¹³C **NMR** (100 MHz, CD₃CN, 25 °C, TMS): δ = 60.14 s (1C, C(7)_{carb}), 55.58 t (1C, J = 136, CH₂S), 47.48 d (1C, J = 152, C(8)H_{carborane}), 38.39 t (1C, J = 127, CH₂), 26.30 t (1C, J = 128, C(7)CH₂); **HRMS (ESI), m/z [M]**: 256.1979 (50%), calcd. 256.1980 (for C₅H₁₉O₂N₁B₉S); **Analysis for Et₃NH.7**: Found C 36.62, H 9.52, N 8.18 Calcd. for B₁₀C₃H₁₅O₂NS: C 37.03, H 9.89, N 7.85.

[7-H₂NSO₂-(CH₂)₄-nido-7,8-C₂B₉H₁₁]Et₃NH (8). MeOH (15 mL) was added to 1-(sulfonamido)butyl-1,2-dicarba-*closo*-dodecaborane (**4**, 1.0 mmol) followed with an excess of Et₃N (0.5 mL, 70 mmol). The methanol solution was stirred and heated at 60 °C for 10 h under reflux. After cooling, volatiles were removed *in vacuo*, and the product was extracted with a ether-ethylacetate mixture (1:1 b.v., 3 x 15 mL). Water (5 mL) was added, and the organic solvents were removed under vacuum pressure. The product was decanted, washed with water, dried, and chromatographed on a silica gel column (25 x 1.5 cm I.D.) using a CH₂Cl₂-CH₃CN solvent mixture (3:1 to 2:1 b.v.) for elution. The final product was a white solid, yield: 0.325 mg (88%), m. p. 118-123 °C; ¹¹B **NMR** (128 MHz, CD₃CN, 25 °C, BF₃.Et₂O): δ = -11.4 d (2B, J = 131, B(9,11)H), -14.23 d (1B, J = 153, B(3)H), -17.77 d (1B, J = 116, B(5)H), -18.48 d (2B,

$J = 107$, $B(2,6)H$), -22.38 d (1B, $J = 137$, $B(4)H$); -33.73 d (1B, $J = 119$, $B(10)H$); -37.58 d (1B, $J = 134$, $B(1)H$); 1H { ^{11}B } NMR (400 MHz, CD_3CN , 25 °C, TMS): $\delta = 5.38$ br. s (2H, NH_2), 3.25 s (1H, $C(7)H_{\text{carborane}}$), 3.09 q (6H, CH_2 $Et_3NH^{(+)}$), 3.00 m (2H, CH_2S), 1.68 m (2H, CH_2), 1.64 t (2H, CH_2), 1.46 s (2H, CH_2), 1.85 s (2H, $B(9,11)H$), 1.48 s (1H, (3)H), 1.21 t (9H, CH_3 $Et_3NH^{(+)}$), 1.15 s (1H, (5)H), 1.02 s (2H, (2,6)H), 1.75 s (1H, (4)H), -0.09 s (1H, (10)H), -0.34 s (1H, (1)H), -2.81 s (1H, μH); ^{13}C NMR (100 MHz, CD_3CN , 25 °C, TMS): $\delta = 60.80$ s (1C, $C(7)_{\text{carb}}$), 46.20 d (1C, $C(8)H_{\text{carb}}$), 54.76 t (1C, CH_2S), 39.55 t (1C, CH_2), 29.75 t (1C, CH_2), 23.98 t (1C, $C(7)CH_2$), 47.68 t (3C, CH_3 $Et_3NH^{(+)}$), 9.23 t (3C, CH_2 $Et_3NH^{(+)}$); HRMS (ESI) m/z [M]: 268.2210 (100%) 270.2136 (52%), calcd. for $C_6H_{20}O_2N_1B_{10}S$: 270.2131 (52%); Analysis for Et_3NH_8 : Found C 38.49, H 9.74, N 7.92 Calcd. for $B_{10}C_3H_{15}O_2NS$: C 38.87, H 10.06, N 7.55. For biological activity tests, the triethylammonium cation present in this salt was replaced with sodium by methathesis.

Protein cloning, expression, and purification. Recombinant CA II and CA IX mimic (CA II containing amino acid substitutions A65S, N67Q, E69T, I91L, F130V, K169E, and L203A) were prepared by heterologous expression in *E. coli* and purified as previously described [34]. The extracellular part of CA IX comprising the PG and CA domains (residues 38-391) and including the amino acid substitution C174S was expressed in HEK 293 cells and purified as previously described [47].

CA inhibition assay. The stopped-flow instrument (Applied Photophysics) has been used for measuring the CA-catalysed CO_2 hydration activity in the presence of inhibitors [48]. The assay buffer consists of 0.2 mM phenol red (pH indicator used in absorbance maximum of 557 nm), 20 mM HEPES-Na (pH 7.5) and 20 mM Na_2SO_4 . Concentration of CA II and CA IX in the enzyme assay was 2.5 nM and 0.5 nM, respectively. To stabilize CA IX, 0.0025 % dodecyl- β -D-maltopyranoside (DDM, Anatrace) was included in the reaction mixture. The substrate (CO_2) concentration in the reaction was 8.5 mM. Rates of the CA-catalysed CO_2 hydration reaction were followed for a period of 30 s at 25 °C. Four traces of the initial 5–10% of the reaction have been used for determining the initial velocity for each inhibitor. The uncatalysed rates were determined in the same manner and subtracted from the total observed rates. Stock solutions of inhibitors (100 mM) were prepared in dimethyl sulfoxide (DMSO) and dilutions up to 100 nM

were made thereafter in DMSO. K_i' values were obtained from dose-response curves recorded for at least six different concentrations of the test compound by the nonlinear least-squares method using an EXCEL spreadsheet fitting the Williams-Morrison equation [49][49]. K_i values were then derived using the Cheng-Prusoff equation [50]. K_M values used in Cheng-Prusoff equation were 9.3 mM for CA II and 7.5 mM for CA IX [51, 52].

Protein crystallization and X-ray data collection. CA IX mimic was used for X-ray studies. Complexes with **3** and **7** were prepared by addition of a 1.1-fold molar excess of inhibitor (dissolved in pure DMSO) to a 25 mg/mL protein solution in 50 mM Tris, pH 7.8. The best crystals were prepared by the vapor-diffusion hanging drop method at 18 °C using a precipitation solution containing 1.6 M sodium citrate, 50 mM Tris-HCl, pH 7.8. Drops containing 2 μ L complex solution were mixed with 1 μ L precipitant solution and equilibrated over a reservoir containing 1 mL precipitant solution. The final DMSO concentration in the drop did not exceed 5% (v/v). Crystals with dimensions of 0.5 mm \times 0.3 mm \times 0.2 mm typically grew within 1-4 weeks. Before data collection, the crystals were soaked for 5–10 s in reservoir solution supplemented with 20% (v/v) sucrose and stored in liquid N₂. Diffraction data at 100 K were collected on BL14.1 operated by the Helmholtz-Zentrum Berlin (HZB) at the BESSY II electron storage ring (Berlin-Adlershof, Germany) [53]. Diffraction data were processed using the XDS suite of programs [54]. Crystal parameters and data collection statistics are summarized in Supplementary Table S1.

Structure determination, refinement, and analyses. Crystal structures of the CA IX mimic in complexes with **3** and **7** were determined by the difference Fourier technique. Coordinates from PDB entry 5OGP were used as a model. Atomic coordinates of inhibitor molecules were generated by quantum mechanical (QM) optimizations in the Turbomole package [55] with the density functional theory (DFT) method using the B-LYP functional and the SVP basis set, augmented with empirical dispersion correction [56]. The geometric library for the inhibitors was generated using the Libcheck program, part of the CCP4 package [57]. Coot [58] was used for inhibitor fitting, model rebuilding, and the addition of water molecules. Refinement was carried out with Refmac5 [59], with 5% of reflections reserved for cross-validation [60].

The structures were first refined with isotropic atomic displacement parameters (ADPs). After adding solvent atoms and zinc ions, building inhibitor molecules in the active site, and exploring several alternate conformations for a number of residues, anisotropic ADPs were refined for nearly all atoms including atoms in the inhibitor molecules (with the exception of spatially overlapping atoms in segments with alternate conformations; oxygen atoms of water molecules with an unrealistic ratio of ellipsoid axes were refined with isotropic ADPs). The quality of the crystallographic model was assessed with MolProbity [61]. The final refinement statistics are summarized in Table S1. All structural figures were created using PyMOL[62]. Atomic coordinates and structure factors for the crystal structures of CA IX mimic in complex with **3** and **7** were deposited in the PDB with accession codes 6T7U and 6T9Z, respectively.

Cell lines. MDCK cells overexpressing CA IX (MDCK-CA IX) and the respective control cells (MDCK-neo) were kindly provided by Prof. Sylvia Pastoreková of the Slovak Academy of Sciences, Bratislava, Slovakia. These cells were maintained as previously described [63]. Mouse breast cancer 4T1-12B-luc cell line stably expressing the luciferase protein was provided by Prof. D. Radioch of The Research Institute of the McGill University Health Centre, Montreal, Canada. The 4T1-12B-luc cells were maintained as previously described [64, 65].

HCT116, HT-29, and Caco-2 colon cancer cells; A549 lung cancer cells; CCRF-CEM and K562 leukemia cell lines; HeLa cervical cancer cells, human skin BJ and lung MRC-5 fibroblasts; and multidrug resistance protein 1 (MDR1)-expressing MDCK (MDCK-MDR1) cells were purchased from ATCC (Middlesex, UK) and maintained according to the manufacturer's recommendation. The multidrug-resistant sublines of CEM (CEM-DNR) and K562 (K562-TAX) expressing the P-glycoprotein and lipoprotein receptor-related proteins, respectively, were generated and maintained as previously described [66]. All cell lines were maintained at 37 °C in a 5% CO₂ atmosphere. For hypoxic induction, cells were cultured in a Heracell 150i humidified incubator (Thermo Fisher Scientific) under a 1% O₂, 94% N₂, and 5% CO₂ atmosphere at 37 °C as described elsewhere [67]. All cell lines were routinely tested for mycoplasma contamination and authenticated weekly or monthly.

Cytotoxicity assay. The cytotoxicity of **3** was determined using a standard 3-(4,5-dimethylthiazol-2-yl)-5-(3-carboxymethoxyphenyl)-2-(4-sulfophenyl)-2H-tetrazolium reduction

assay on a robotic high-throughput screening platform (HighResBio, Boston, MA) following treatment of cells for 3-7 days. The IC_{50} values were calculated from the appropriate dose-response curves with Dotmatics (San Diego, CA, USA).

Spheroid generation and drug treatment. Spheroids of HCT116 and HT-29 cells were generated as previously described [68]. For determining the effect of **3** on spheroid size, 7-day-old spheroids were treated with different concentrations of **3** for 3-7 days. Spheroids were imaged in a high-content imaging system (Yokogawa Electric Corporation, Tokyo, Japan), and the images were analyzed using an in-house algorithm as previously described [69]. The effect of **3** on spheroid size was calculated as a percentage of untreated controls, and the IC_{50} values were determined from the respective dose-response curves using GraphPad Prism Software (version 7; GraphPad Prism, San Diego, CA).

Whole-mount immunostaining and Western blot. To perform whole-mount immunostaining of spheroids, ten-day-old spheroids were treated with **3** ($1\times$ inhibitor dose based on day-7 IC_{50} concentrations) for 3 days under standard cell culture conditions. Spheroids were processed for whole-mount immunostaining and imaging using a Lightsheet Z.1 microscope (Carl Zeiss) as previously described [70]. Images were processed using ZEN 2012 Black Edition imaging software (Carl Zeiss).

For Western blot, spheroids were treated with $0.5\times$, $1\times$ and $2\times$ day-7 IC_{50} concentrations of **3** for 3 days. Following drug treatment, 30-40 MCSs were collected, dispersed into single cells using Accutase[®] Cell Detachment Solution (Sigma-Aldrich, Prague, Czech Republic), and lysed in RIPA cell lysis buffer containing protease inhibitors by sonication on ice. Protein lysates were then separated by a standard gel electrophoresis protocol and analyzed by Western blotting for CA IX expression changes as described previously [30]

Doxorubicin penetration into HT-29 spheroids. To determine the penetration of DOX, a prototypical fluorescent anticancer drug, in the presence of **3**, time-lapse images of spheroids were acquired with a Lightsheet Z.1 microscope (Carl Zeiss) as described previously [30].

***In vitro* pharmacology.** Compound **3** was assayed *in vitro* for human plasma and liver microsomal stability. It was subjected to a parallel artificial membrane permeability assay (PAMPA) and cellular permeability models of gastrointestinal resorption and the blood-brain barrier using Caco-2 and MDR1-MCDK cells as previously described [71]. Samples were analyzed in an Agilent RapidFire 300 High-Throughput Mass Spectrometry System (RF-MS; Agilent, Wakefield, MA) with subsequent detection in a Qtrap 5500 mass spectrometer (AB Sciex, Concord, Canada). See Supporting Information for details.

***In vivo* pharmacokinetics.** Compounds **2** and **3** and sodium salts **6** and **7** were administered intraperitoneally to female NMRI mice at maximum and half-maximum tolerated doses (MTD 125 mg/kg and ½MTD 62.5 mg/kg). Compounds **2**, **6**, and **7** were administered in a solution of 50% PEG400. Compound **3** was dissolved and formulated in a 90% saline and 10% DMSO solution. Animals were sacrificed under anesthesia by bleeding from the brachial plexus after 0.5, 1, 3, 6, 9, 12, 24 and 36 h (3 mice per group). Blood was collected on ice and processed for serum separation within 60 min after sampling. Mouse brains and other tissues were removed from the body and deep-frozen. Brains were homogenized with a high-speed stainless steel mixer. The boron content in serum and brain samples was determined using electrothermal vaporization (ETV) coupled with inductively-coupled plasma optical emission spectrometry (ICP-OES). Homogenized samples, including serum samples, were weighed in a graphite boat and dried on an electrical hot plate at 105 °C. The ETV method involves placing a few milligrams of sample material into a graphite furnace, where the material is vaporized, halogenated using a modifier gas, transferred to ICP-OES and introduced into plasma as a dry aerosol. An ETV 4000c System electrothermal vaporization device (Spectral Systems, Fürstfeldbruck, Germany) was used for sample introduction. A special software module enables the processing of the transient signal of the tracked element wavelengths from ICP synchronized with the ETV-temperature program. As ICP-OES spectrometer, we used a Spectro Arcos ICP with radial plasma observation (Spectro Analytical Instruments, Kleve, Germany). The Spectro Arcos features a Paschen-Runge optic mount that enables simultaneous spectral analysis in the wavelength range from 130 to 770 nm. The detection limit of the method was 0.010 ppm for boron (typical RSD ≤ 3%, 3 replicates per measurement).

Anti-tumor activity in mice xenografts. Human colorectal cancer HT-29 cells were xenotransplanted (1.5×10^6 cells/ injection) subcutaneously on both sides of the chest of SCID mice (Envigo, Huntingdon, United Kingdom). Mouse breast cancer 4T1 cells were xenotransplanted (1×10^6 cells/injection) orthotopically into the seventh mammary fat pad of BALB/c mice (Envigo, Huntingdon, United Kingdom). Animals were randomly enrolled into study groups and treated with **3** when the optimal tumor size was reached. The compounds were repeatedly intraperitoneally administered on days 1-5, 8-12, and 15-19. Compound **3** was administered once per day at doses of 62.5 mg/ kg and 38 mg/kg, respectively. The animals were monitored for an overall period of 24 or 33 days following compound administration. The size of the tumor was recorded using a caliper, and the volume was calculated using a modified ellipsoid formula $[(L \times W^2)/ 2]$, where L and W denote length and width, respectively]. Animals were housed in specific pathogen-free conditions with a 12 h light/night regime and clinically examined daily for water and food *ad libitum*. All animal procedures were approved by the Animal Ethics Committee of the Faculty of Medicine and Dentistry, Palacky University Olomouc, Czech Republic.

Statistical analysis All statistical analyses were performed using GraphPad Prism software (GraphPad Prism), and differences were considered significant at $p < 0.05$.

Supporting material contains details on chemical syntheses, Figures S1-S3: Inhibition curves. Table S1: Diffraction data collection and refinement statistics, Figure S4: Details of structure of **3** and **7** bound to the CA IX active site, Figure S5: Pharmacokinetic profiles of carborane compounds, Supplementary references and NMR spectra for all compounds.

ACKNOWLEDGMENT

This work was supported by the Czech Science Foundation, Project Nos. 18-27648S and 15-05677S (early stages of this study); the Technology Agency of the Czech Republic, Project TE01020028; and PPLZ Project No. 1827648S (to S. El A.) from the Academy of Sciences of the Czech Republic; and the Ministry of Education of the Czech Republic, Grants CZ.02.1.01/0.0/0.0/ 16_019/0000868 and EATRIS-CZ LM2015064; and Internal Grant Agency

of Palacky University (IGA LF_2020_007) The use of beamlines MX14.1 and MX14.2 operated by the Helmholtz-Zentrum Berlin at the BESSY II electron storage ring (Berlin-Adlershof, Germany) to collect diffraction data is gratefully acknowledged.

REFERENCES

1. Semenza, G. L. (2014) Oxygen sensing, hypoxia-inducible factors, and disease pathophysiology, *Annu Rev Pathol.* **9**, 47-71.
2. Warburg, O. (1956) On respiratory impairment in cancer cells, *Science.* **124**, 269-70.
3. Wojtkowiak, J. W., Verduzco, D., Schramm, K. J. & Gillies, R. J. (2011) Drug resistance and cellular adaptation to tumor acidic pH microenvironment, *Mol Pharm.* **8**, 2032-8.
4. Good, J. S. & Harrington, K. J. (2013) The hallmarks of cancer and the radiation oncologist: updating the 5Rs of radiobiology, *Clin Oncol (R Coll Radiol).* **25**, 569-77.
5. Pastorekova, S., Ratcliffe, P. J. & Pastorek, J. (2008) Molecular mechanisms of carbonic anhydrase IX-mediated pH regulation under hypoxia, *BJU Int.* **101 Suppl 4**, 8-15.
6. Swietach, P., Wigfield, S., Cobden, P., Supuran, C. T., Harris, A. L. & Vaughan-Jones, R. D. (2008) Tumor-associated carbonic anhydrase 9 spatially coordinates intracellular pH in three-dimensional multicellular growths, *J Biol Chem.* **283**, 20473-83.
7. McDonald, P. C., Chafe, S. C. & Dedhar, S. (2016) Overcoming Hypoxia-Mediated Tumor Progression: Combinatorial Approaches Targeting pH Regulation, Angiogenesis and Immune Dysfunction, *Front Cell Dev Biol.* **4**, 27.
8. Pastorekova, S., Parkkila, S., Parkkila, A. K., Opavsky, R., Zelnik, V., Saarnio, J. & Pastorek, J. (1997) Carbonic anhydrase IX, MN/CA IX: analysis of stomach complementary DNA sequence and expression in human and rat alimentary tracts, *Gastroenterology.* **112**, 398-408.
9. Chia, S. K., Wyckoff, C. C., Watson, P. H., Han, C., Leek, R. D., Pastorek, J., Gatter, K. C., Ratcliffe, P. & Harris, A. L. (2001) Prognostic significance of a novel hypoxia-regulated marker, carbonic anhydrase IX, in invasive breast carcinoma, *Journal of clinical oncology : official journal of the American Society of Clinical Oncology.* **19**, 3660-8.
10. Koukourakis, M. I., Giatromanolaki, A., Sivridis, E., Simopoulos, K., Pastorek, J., Wyckoff, C. C., Gatter, K. C. & Harris, A. L. (2001) Hypoxia-regulated carbonic anhydrase-9 (CA9) relates to poor vascularization and resistance of squamous cell head and neck cancer to chemoradiotherapy, *Clinical cancer research : an official journal of the American Association for Cancer Research.* **7**, 3399-403.
11. Loncaster, J. A., Harris, A. L., Davidson, S. E., Logue, J. P., Hunter, R. D., Wyckoff, C. C., Pastorek, J., Ratcliffe, P. J., Stratford, I. J. & West, C. M. (2001) Carbonic anhydrase (CA IX) expression, a potential new intrinsic marker of hypoxia: correlations with tumor oxygen measurements and prognosis in locally advanced carcinoma of the cervix, *Cancer Res.* **61**, 6394-9.
12. Bui, M. H., Seligson, D., Han, K. R., Pantuck, A. J., Dorey, F. J., Huang, Y., Horvath, S., Leibovich, B. C., Chopra, S., Liao, S. Y., Stanbridge, E., Lerman, M. I., Palotie, A., Figlin, R. A. & Belldegrun, A. S. (2003) Carbonic anhydrase IX is an independent predictor of survival in advanced renal clear cell carcinoma: implications for prognosis and therapy, *Clinical cancer research : an official journal of the American Association for Cancer Research.* **9**, 802-11.
13. Haapasalo, J. A., Nordfors, K. M., Hilvo, M., Rantala, I. J., Soini, Y., Parkkila, A. K., Pastorekova, S., Pastorek, J., Parkkila, S. M. & Haapasalo, H. K. (2006) Expression of carbonic

anhydrase IX in astrocytic tumors predicts poor prognosis, *Clinical cancer research : an official journal of the American Association for Cancer Research*. **12**, 473-7.

14. Brennan, D. J., Jirstrom, K., Kronblad, A., Millikan, R. C., Landberg, G., Duffy, M. J., Ryden, L., Gallagher, W. M. & O'Brien, S. L. (2006) CA IX is an independent prognostic marker in premenopausal breast cancer patients with one to three positive lymph nodes and a putative marker of radiation resistance, *Clinical cancer research : an official journal of the American Association for Cancer Research*. **12**, 6421-31.

15. Cianchi, F., Vinci, M. C., Supuran, C. T., Peruzzi, B., De Giuli, P., Fasolis, G., Perigli, G., Pastorekova, S., Papucci, L., Pini, A., Masini, E. & Puccetti, L. (2010) Selective Inhibition of Carbonic Anhydrase IX Decreases Cell Proliferation and Induces Ceramide-Mediated Apoptosis in Human Cancer Cells, *Journal of Pharmacology and Experimental Therapeutics*. **334**, 710-719.

16. Supuran, C. T. & Winum, J. Y. (2015) Carbonic anhydrase IX inhibitors in cancer therapy: an update, *Future Medicinal Chemistry*. **7**, 1407-1414.

17. Carta, F., Supuran, C. T. & Scozzafava, A. (2014) Sulfonamides and their isosters as carbonic anhydrase inhibitors, *Future Medicinal Chemistry*. **6**, 1149-1165.

18. Kazokaite, J., Aspatwar, A., Parkkila, S. & Matulis, D. (2017) An update on anticancer drug development and delivery targeting carbonic anhydrase IX, *PeerJ*. **5**, e4068.

19. Lou, Y. M., McDonald, P. C., Oloumi, A., Chia, S., Ostlund, C., Ahmadi, A., Kyle, A., Keller, U. A. D., Leung, S., Huntsman, D., Clarke, B., Sutherland, B. W., Waterhouse, D., Bally, M., Roskelley, C., Overall, C. M., Minchinton, A., Pacchiano, F., Carta, F., Scozzafava, A., Touisni, N., Winum, J. Y., Supuran, C. T. & Dedhar, S. (2011) Targeting Tumor Hypoxia: Suppression of Breast Tumor Growth and Metastasis by Novel Carbonic Anhydrase IX Inhibitors, *Cancer Research*. **71**, 3364-3376.

20. Pacchiano, F., Carta, F., McDonald, P. C., Lou, Y. M., Vullo, D., Scozzafava, A., Dedhar, S. & Supuran, C. T. (2011) Ureido-Substituted Benzenesulfonamides Potently Inhibit Carbonic Anhydrase IX and Show Antimetastatic Activity in a Model of Breast Cancer Metastasis, *Journal of Medicinal Chemistry*. **54**, 1896-1902.

21. Pinard, M. A., Mahon, B. & McKenna, R. (2015) Probing the Surface of Human Carbonic Anhydrase for Clues towards the Design of Isoform Specific Inhibitors, *Biomed Research International*, 15.

22. Grimes, R. N. (2011) *Carboranes, 2nd Ed.*, Academic Press Publications (Elsevier, Inc.), London- Amsterdam- Burlington- San Diego- Oxford.

23. Lesnikowski, Z. J. (2016) Challenges and Opportunities for the Application of Boron Clusters in Drug Design, *Journal of Medicinal Chemistry*. **59**, 7738-7758.

24. Sibrian-Vazquez, M., Hao, E., Jensen, T. J. & Vicente, M. G. H. (2006) *Bioconjugate Chemistry*. **17**, 928.

25. Valliant, J. F., Guenther, K. J., King, A. S., Morel, P., Schaffer, P., Sogbein, O. O. & Stephenson, K. A. (2002) The medicinal chemistry of carboranes, *Coordination Chemistry Reviews*. **232**, 173-230.

26. Sivaev, I. B. & Bregadze, V. I. (2009) Polyhedral Boranes for Medical Applications: Current Status and Perspectives *European Journal of Inorganic Chemistry*. **2009**, 1433-1450.

27. Satapathy, R., Dash, B. P., Maguire, J. A. & Hosmane, N. S. (2010) NEW DEVELOPMENTS IN THE MEDICINAL CHEMISTRY OF CARBORANES *Collect Czech Chem Commun*. **75**, 995-1022.

28. Issa, F., Kassiou, M. & Rendina, M. (2011) Boron in Drug Discovery: Carboranes as Unique Pharmacophores in Biologically Active Compounds, *Chemical Reviews*. **111**, 5701-5722.
29. Mader, P., Pecina, A., Cigler, P., Lepsik, M., Sicha, V., Hobza, P., Gruner, B., Fanfrlik, J., Brynda, J. & Rezacova, P. (2014) Carborane-Based Carbonic Anhydrase Inhibitors: Insight into CAII/CAIX Specificity from a High-Resolution Crystal Structure, Modeling, and Quantum Chemical Calculations, *Biomed Res Int*.
30. Brynda, J., Mader, P., Šícha, V., Fábry, M., Poncová, K., Bakardiev, M., Gruner, B., Cígler, P. & Řezáčová, P. (2013) Carborane-Based Carbonic Anhydrase Inhibitors, *Angew Chem, Intl Ed Eng*. **52**, 13760-13763.
31. Gruner, B., Brynda, J., Das, V., Sicha, V., Stepankova, J., Nektivinda, J., Holub, J., Pospisilova, K., Fabry, M., Pacht, P., Kral, V., Kugler, M., Masek, V., Medvedikova, M., Matejkova, S., Nova, A., Liskova, B., Gurska, S., Dzubak, P., Hajduch, M. & Rezacova, P. (2019) Metallacarborane Sulfamides: Unconventional, Specific, and Highly Selective Inhibitors of Carbonic Anhydrase IX, *J Med Chem*. **62**, 9560-9575.
32. Supuran, C. T. (2017) Advances in structure-based drug discovery of carbonic anhydrase inhibitors, *Expert Opin Drug Discov*. **12**, 61-88.
33. Yoo, Y., Hwang, J. W. & Do, Y. (2001) Facile and mild deboronation of o-carboranes using cesium fluoride, *Inorganic Chemistry*. **40**, 568-+.
34. Pinard, M. A., Boone, C. D., Rife, B. D., Supuran, C. T. & McKenna, R. (2013) Structural study of interaction between brinzolamide and dorzolamide inhibition of human carbonic anhydrases, *Bioorganic & Medicinal Chemistry*. **21**, 7210-7215.
35. Winum, J. Y., Scozzafava, A., Montero, J. L. & Supuran, C. T. (2006) Therapeutic potential of sulfamides as enzyme inhibitors, *Medicinal Research Reviews*. **26**, 767-792.
36. De Simone, G., Langella, E., Esposito, D., Supuran, C. T., Monti, S. M., Winum, J. Y. & Alterio, V. (2017) Insights into the binding mode of sulphamates and sulphamides to hCA II: crystallographic studies and binding free energy calculations, *Journal of Enzyme Inhibition and Medicinal Chemistry*. **32**, 1002-1011.
37. Di Fiore, A., Monti, S. M., Innocenti, A., Winum, J.-Y., De Simone, G. & Supuran, C. T. (2010) Carbonic anhydrase inhibitors: Crystallographic and solution binding studies for the interaction of a boron-containing aromatic sulfamide with mammalian isoforms I-XV, *Bioorganic & Medicinal Chemistry Letters*. **20**, 3601-3605.
38. Fanfrlik, J., Lepsik, M., Horinek, D., Havlas, Z. & Hobza, P. (2006) Interaction of carboranes with biomolecules: formation of dihydrogen bonds, *Chemphyschem*. **7**, 1100-5.
39. Pecina, A., Lepsik, M., Rezac, J., Brynda, J., Mader, P., Rezacova, P., Hobza, P. & Fanfrlik, J. (2013) QM/MM calculations reveal the different nature of the interaction of two carborane-based sulfamide inhibitors of human carbonic anhydrase II, *J Phys Chem B*. **117**, 16096-104.
40. Das, V., Bruzzese, F., Konecny, P., Iannelli, F., Budillon, A. & Hajduch, M. (2015) Pathophysiologically relevant in vitro tumor models for drug screening, *Drug Discov Today*. **20**, 848-55.
41. Csaderova, L., Debreova, M., Radvak, P., Stano, M., Vrestiakova, M., Kopacek, J., Pastorekova, S. & Svastova, E. (2013) The effect of carbonic anhydrase IX on focal contacts during cell spreading and migration, *Front Physiol*. **4**, 271.
42. Yang, J. S., Lin, C. W., Hsieh, Y. H., Chien, M. H., Chuang, C. Y. & Yang, S. F. (2017) Overexpression of carbonic anhydrase IX induces cell motility by activating matrix metalloproteinase-9 in human oral squamous cell carcinoma cells, *Oncotarget*. **8**, 83088-83099.

43. Ji, T., Lang, J., Wang, J., Cai, R., Zhang, Y., Qi, F., Zhang, L., Zhao, X., Wu, W., Hao, J., Qin, Z., Zhao, Y. & Nie, G. (2017) Designing Liposomes To Suppress Extracellular Matrix Expression To Enhance Drug Penetration and Pancreatic Tumor Therapy, *ACS Nano*. **11**, 8668-8678.
44. Gerweck, L. E. & Seetharaman, K. (1996) Cellular pH gradient in tumor versus normal tissue: potential exploitation for the treatment of cancer, *Cancer Res*. **56**, 1194-8.
45. McIntyre, A., Patiar, S., Wigfield, S., Li, J. L., Ledaki, I., Turley, H., Leek, R., Snell, C., Gatter, K., Sly, W. S., Vaughan-Jones, R. D., Swietach, P. & Harris, A. L. (2012) Carbonic anhydrase IX promotes tumor growth and necrosis in vivo and inhibition enhances anti-VEGF therapy, *Clinical cancer research : an official journal of the American Association for Cancer Research*. **18**, 3100-11.
46. Beall, H. & Gaines, D. F. (1998) Reactions of 6,9-bis(dimethyl sulfide)decaborane(14), 6,9-(CH₃)₂S (2)B₁₀H₁₂: Mechanistic considerations, *Inorganic Chemistry*. **37**, 1420-+.
47. Pospisilova, K., Knedlik, T., Sacha, P., Kostka, L., Schimer, J., Brynda, J., Kral, V., Cigler, P., Navratil, V., Etrych, T., Subr, V., Kugler, M., Fabry, M., Rezacova, P. & Konvalinka, J. (2019) Inhibitor-Polymer Conjugates as a Versatile Tool for Detection and Visualization of Cancer-Associated Carbonic Anhydrase Isoforms, *Acs Omega*. **4**, 6746-6756.
48. Khalifah, R. G. (1971) CARBON DIOXIDE HYDRATION ACTIVITY OF CARBONIC ANHYDRASE .1. STOP-FLOW KINETIC STUDIES ON NATIVE HUMAN ISOENZYME-B AND ISOENZYME-C, *Journal of Biological Chemistry*. **246**, 2561-&.
49. Morrisson, J. W. M. & Williams, J. F. (1979) The kinetics of reversible tight-binding inhibition, *Methods Enzymol*. **63**, 437-467.
50. Yung-Chi, C. & Prusoff, W. H. (1973) Relationship between the inhibition constant (KI) and the concentration of inhibitor which causes 50 per cent inhibition (I50) of an enzymatic reaction, *Biochemical Pharmacology*. **22**, 3099-3108.
51. Innocenti, A., Scozzafava, A., Parkkila, S., Puccetti, L., De Simone, G. & Supuran, C. T. (2008) Investigations of the esterase, phosphatase, and sulfatase activities of the cytosolic mammalian carbonic anhydrase isoforms I, II, and XIII with 4-nitrophenyl esters as substrates, *Bioorganic & Medicinal Chemistry Letters*. **18**, 2267-2271.
52. Hilvo, M., Baranauskiene, L., Salzano, A. M., Scaloni, A., Matulis, D., Innocenti, A., Scozzafava, A., Monti, S. M., Di Fiore, A., De Simone, G., Lindfors, M., Janis, J., Valjakka, J., Pastorekova, S., Pastorek, J., Kulomaa, M. S., Nordlund, H. R., Supuran, C. T. & Parkkila, S. (2008) Biochemical characterization of CA IX, one of the most active carbonic anhydrase isozymes, *J Biol Chem*. **283**, 27799-809.
53. Mueller, U., Darowski, N., Fuchs, M. R., Forster, R., Hellmig, M., Paithankar, K. S., Puhlinger, S., Steffien, M., Zocher, G. & Weiss, M. S. (2012) Facilities for macromolecular crystallography at the Helmholtz-Zentrum Berlin, *Journal of Synchrotron Radiation*. **19**, 442-449.
54. Kabsch, W. (2010) Integration, scaling, space-group assignment and post-refinement, *Acta Crystallographica Section D-Biological Crystallography*. **66**, 133-144.
55. Ahlrichs, R., Bar, M., Haser, M., Horn, H. & Kolmel, C. (1989) Electronic-Structure Calculations on Workstation Computers - the Program System Turbomole, *Chem Phys Lett*. **162**, 165-169.
56. Jurecka, P., Cerny, J., Hobza, P. & Salahub, D. R. (2007) Density functional theory augmented with an empirical dispersion term. Interaction energies and geometries of 80

noncovalent complexes compared with ab initio quantum mechanics calculations, *J Comput Chem.* **28**, 555-569.

57. Winn, M. D., Ballard, C. C., Cowtan, K. D., Dodson, E. J., Emsley, P., Evans, P. R., Keegan, R. M., Krissinel, E. B., Leslie, A. G., McCoy, A., McNicholas, S. J., Murshudov, G. N., Pannu, N. S., Potterton, E. A., Powell, H. R., Read, R. J., Vagin, A. & Wilson, K. S. (2011) Overview of the CCP4 suite and current developments, *Acta Crystallogr D Biol Crystallogr.* **67**, 235-42.

58. Emsley, P. & Cowtan, K. (2004) Coot: model-building tools for molecular graphics, *Acta Crystallogr D Biol Crystallogr.* **60**, 2126-32.

59. Vagin, A. A., Steiner, R. A., Lebedev, A. A., Potterton, L., McNicholas, S., Long, F. & Murshudov, G. N. (2004) REFMAC5 dictionary: organization of prior chemical knowledge and guidelines for its use, *Acta Crystallogr D Biol Crystallogr.* **60**, 2184-95.

60. Brunger, A. T., Kuriyan, J. & Karplus, M. (1987) Crystallographic R factor refinement by molecular dynamics, *Science.* **235**, 458-60.

61. Williams, C. J., Headd, J. J., Moriarty, N. W., Prisant, M. G., Videau, L. L., Deis, L. N., Verma, V., Keedy, D. A., Hintze, B. J., Chen, V. B., Jain, S., Lewis, S. M., Arendall, W. B., 3rd, Snoeyink, J., Adams, P. D., Lovell, S. C., Richardson, J. S. & Richardson, D. C. (2018) MolProbity: More and better reference data for improved all-atom structure validation, *Protein Sci.* **27**, 293-315.

62. DeLano, W. L. (2009) in *The PyMOL Molecular Graphics System DeLano Scientific, San Carlos, CA.*

63. Svastova, E., Zilka, N., Zat'ovicova, M., Gibadulinova, A., Ciampor, F., Pastorek, J. & Pastorekova, S. (2003) Carbonic anhydrase IX reduces E-cadherin-mediated adhesion of MDCK cells via interaction with beta-catenin, *Exp Cell Res.* **290**, 332-45.

64. Ditte, P., Dequiedt, F., Svastova, E., Hulikova, A., Ohradanova-Repic, A., Zatovicova, M., Csaderova, L., Kopacek, J., Supuran, C. T., Pastorekova, S. & Pastorek, J. (2011) Phosphorylation of carbonic anhydrase IX controls its ability to mediate extracellular acidification in hypoxic tumors, *Cancer Res.* **71**, 7558-67.

65. Xu, Y. Z., Heravi, M., Thuraisingam, T., Di Marco, S., Muanza, T. & Radzioch, D. (2010) Brg-1 mediates the constitutive and fenretinide-induced expression of SPARC in mammary carcinoma cells via its interaction with transcription factor Sp1, *Mol Cancer.* **9**, 210.

66. Noskova, V., Dzubak, P., Kuzmina, G., Ludkova, A., Stehlik, D., Trojanec, R., Janostakova, A., Korinkova, G., Mihal, V. & Hajduch, M. (2002) In vitro chemoresistance profile and expression/function of MDR associated proteins in resistant cell lines derived from CCRF-CEM, K562, A549 and MDA MB 231 parental cells, *Neoplasma.* **49**, 418-425.

67. Rehulka, J., Annadurai, N., Frydrych, I., Dzubak, P., Miller, J. H., Hajduch, M. & Das, V. (2018) Peloruside A-Induced Cell Death in Hypoxia Is p53 Dependent in HCT116 Colorectal Cancer Cells, *J Nat Prod.* **81**, 634-640.

68. Das, V., Furst, T., Gurska, S., Dzubak, P. & Hajduch, M. (2016) Reproducibility of Uniform Spheroid Formation in 384-Well Plates: The Effect of Medium Evaporation, *Journal of Biomolecular Screening.* **21**, 923-930.

69. Das, V., Furst, T., Gurska, S., Dzubak, P. & Hajduch, M. (2017) Evaporation-reducing Culture Condition Increases the Reproducibility of Multicellular Spheroid Formation in Microtiter Plates, *Jove-Journal of Visualized Experiments.*

70. Agrawal, K., Das, V., Otmar, M., Krecmerova, M., Dzubak, P. & Hajduch, M. (2017) Cell-based DNA demethylation detection system for screening of epigenetic drugs in 2D, 3D, and xenograft models, *Cytometry Part A*. **91A**, 133-143.
71. Perlikova, P., Rylova, G., Naus, P., Elbert, T., Tloustova, E., Bourderioux, A., Slavetinska, L. P., Motyka, K., Dolezal, D., Znojek, P., Nova, A., Harvanova, M., Dzubak, P., Siller, M., Hlavac, J., Hajduch, M. & Hocek, M. (2016) 7-(2-Thienyl)-7-Deazaadenosine (AB61), a New Potent Nucleoside Cytostatic with a Complex Mode of Action, *Mol Cancer Ther.* **15**, 922-37.

Highlights

- Carborane alkylsulfonamides are potent and selective inhibitors of human CA IX
- Inhibitory potency and specificity is driven by a length of alkyl linker
- Selective inhibition of CA IX with a subnanomolar K_i value
- Moderate effect on tumor size in mice
- Favorable ADME properties and pharmacokinetics in mice

Declaration of interests

The authors declare that they have no known competing financial interests or personal relationships that could have appeared to influence the work reported in this paper.

The authors declare the following financial interests/personal relationships which may be considered as potential competing interests:

The authors declare the following competing financial interest(s): B. Gruner, J. Brynda, V. Sicha, J. Holub, P. Dzubak, M. Hajduch, and P. Rezacova are inventors of a United States Patent, Pat. No. 9,290,529 B2, issued on Date Mar. 22, 2016 that covers the title compounds.